Fluorescence Probing of Temperature-Dependent Dynamics and Friction in Ionic Liquid Local Environments†

Alison M. Funston,‡ Tatiana A. Fadeeva,§ James F. Wishart,*,|| and Edward W. Castner, Jr.*,§

School of Chemistry, University of Melbourne, Melbourne, Australia, Department of Chemistry and Chemical Biology, Rutgers, The State University of New Jersey, Piscataway, New Jersey 08854-8087, and Chemistry Department, Brookhaven National Laboratory, Building 555A, Upton, New York 11973-5000

Received: December 4, 2006; In Final Form: March 21, 2007

The solvation dynamics and local orientational friction for a series of four ionic liquids have been probed using coumarin 153 (C153) as a function of temperature. These ionic liquids are comprised of nonaromatic organic cations paired with a common anion, bis(trifluoromethylsulfonyl)imide (NTf_2^-). The specific liquids are as follows: *N*-methyl-tri-*N*-butylammonium NTf_2^- (N_{1444}^+/NTf_2^-), *N*-hexyl-tri-*N*-butylammonium NTf_2^- (N_{6444}^+/NTf_2^-), *N*-methyl-*N*-butylpyrrolidinium NTf_2^- ($Pyrr_{14}^+/NTf_2^-$), and *N*-methyl-*N*-ethoxyethylpyrrolidinium NTf_2^- ($Pyrr_{1(2O2)}^+/NTf_2^-$). The observed solvation dynamics and fluorescence depolarization dynamics occur over a broad range of time scales that can only be adequately fit by functions including three or more exponential components. Stretched exponential distributions cannot adequately fit our data. The solvation and reorientational dynamics of the C153 probe are studied over a range of temperatures from 278.2 to 353.2 K. For both the solvation dynamics and the probe reorientational dynamics, the observed temperature dependence is well fit by a Vogel−Tammann−Fulcher law. To correlate the observed microscopic dynamics with macroscopic physical properties, temperature-dependent viscosities are also measured. Differential scanning calorimetry is used to study the thermodynamics of the phase transitions from the liquid to supercooled liquid to glassy states. For the two tetraalkylammonium liquids, the observed melting transitions occur near 300 K, so we are able to study the dynamics in a clearly supercooled regime. Very long time scale orientational relaxation time constants dynamics on the order of 100 ns are observed in the C153 fluorescence anisotropy. These are interpreted to arise from long-lived local structures in the environment surrounding the C153 probe.

Introduction

Research into the chemical and physical properties of ionic liquids (ILs) is leading to rapid progress in many areas, especially in understanding their complex local structures[1−5] and dynamics.[6−20] Ionic liquids are rather different from common organic solvents in a number of ways. At a practical level, they have much higher viscosities[21−26] and boiling points[27] as well as much larger electrochemical windows and conductivities.[24,26,28−32] Many ionic liquids do not show a clear melting transition, as crystallization is not always observed. For those liquids that do show a melting transition, the melting temperature is frequently above ambient, meaning that room-temperature ILs can sometimes be supercooled liquids. Computer simulations from several groups have shown ionic liquids to be nanostructured.[3−5,33] Triolo, et al. have used X-ray diffraction to demonstrate nanoscale segregation in ionic liquids comprised of 1-alkyl-3-methylimidazolium cations and either chloride or tetrafluoroborate anions.[34] A number of pieces of evidence from both experiment and computer simulation show that there is substantial conformational heterogeneity for either the ionic liquid cations,[2,35,36] anions,[37−42] or both. In addition to the evidence for nanostructural organization, there is also NMR and conductivity evidence for the existence of persistent clusters in the liquid.[24,26,28]

In this paper, we will discuss our work in understanding the relevant timescales for reorganization dynamics of four ionic liquids using time-resolved fluorescence spectroscopy. Structures of the component ions for the four liquids we have studied are shown in Figure 1. Specifically, the liquids studied are: *N*-methyl-tri-*N*-butylammonium bis(trifluoromethylsulfonyl)-imide (N_{1444}^+/NTf_2^-), *N*-hexyl-tri-*N*-butylammonium NTf_2^- (N_{6444}^+/NTf_2^-), *N*-methyl-*N*-butylpyrrolidinium NTf_2^- ($Pyrr_{14}^+/NTf_2^-$), and *N*-methyl-*N*-ethoxyethylpyrrolidinium NTf_2^- ($Pyrr_{1(2O2)}^+/NTf_2^-$). The four ILs discussed herein are all based on nonaromatic cations paired with the highly flexible NTf_2^- anion. The NTf_2^- anion is chosen because it provides ILs with low room-temperature viscosities, high thermal stability, and broad electrochemical windows.

Spectroscopic methods have been widely used to probe the dynamics in ionic liquids. Understanding the dynamics in the neat ionic liquids is achieved through NMR,[24,26,28] optical Kerr effect,[20,37−40,43−47] and TeraHertz spectroscopies,[48,49] as well as by inelastic neutron scattering methods.[50,51] For an understanding of the dynamics most directly relevant to charge-transfer processes and solvation during chemical reactions, fluorescence spectroscopy on a probe molecule in ionic solution is frequently used.

Time-resolved fluorescence spectroscopy has been widely used for more than two decades to probe solvation dynamics by measuring the dynamic evolution of the emission spectrum of a suitable solvatochromic probe molecule such as coumarin 153 (C153, also shown in Figure 1).[52,53] This method is

† Part of the special issue "Physical Chemistry of Ionic Liquids".
* To whom correspondence should be addressed.
‡ University of Melbourne.
§ Rutgers, The State University of New Jersey.
|| Brookhaven National Laboratory.

10.1021/jp068298o CCC: $37.00
Published on Web 04/18/2007

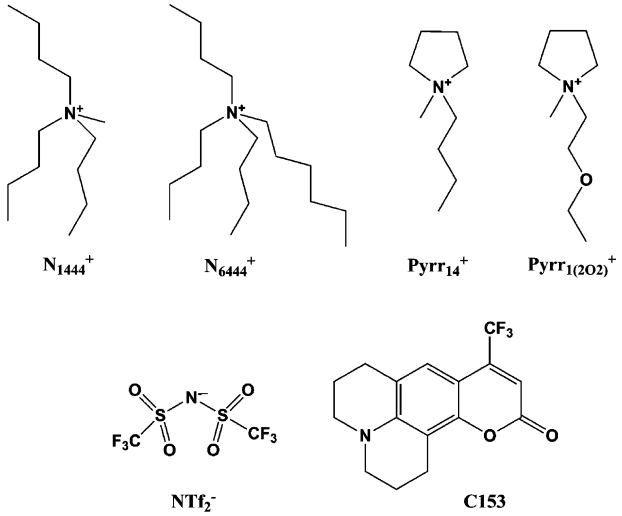

Figure 1. Structures of the four ionic liquid cations: N_{1444}^+, N_{6444}^+, $Pyrr_{14}^+$, and $Pyrr_{1(2O2)}^+$, together with the ionic liquid anion NTf_2^- and the fluorescence probe molecule coumarin 153 (C153).

often referred to as the time-dependent fluorescence Stokes shift (TDFSS). Time-resolved fluorescence anisotropy has also been widely used to probe the friction of the local environment by correlating the dynamics of the anisotropy decay with the reorientational time-correlation function of the fluorescent probe.[54−56] It is frequently convenient to use the same solvatochromic probe for both the TDFSS solvation dynamics experiment and the fluorescence anisotropy experiment. C153 has been well characterized for both purposes.[53,57]

Several groups have previously studied ionic liquids using time-resolved fluorescence methods.[6−9,11−14,19,58−66] In particular, two of the four liquids we report on here have been studied previously. Arzhantsev et al. have studied the solvation dynamics of N_{1444}^+/NTf_2^-[58] and Mandal and Samanta have studied the solvation dynamics of $Pyrr_{14}^+/NTf_2^-$.[14] As discussed below, our results are in qualitative agreement but show minor though not insignificant differences compared to the prior work. A number of probe molecules have been used, including the one we report on here, C153. For a given ionic liquid, the dynamic solvation of the solvatochromic probe has been shown to be highly dependent upon the structure of the probe itself.[6,9,63,67] In a number of cases, specific intermolecular interactions between the probe and the ionic liquid have been postulated.[6,64]

To date detailed investigations have predominantly focused either on one liquid or one class of ionic liquids, most often imidazolium salts. The solvation dynamics observed in the imidazolium ionic liquids occur on two timescales, one in the picosecond regime and the other in the nanosecond regime.[6−9,11,58,63] The slower decay is highly nonexponential and has been fit to a stretched exponential (or Kohlrausch) function[9,58] or to a sum of two exponential decays.[7,8,11,13] Generally, this longer time scale relaxation has been ascribed to the large scale reorganization of the solvent structure. Both translational motion of one of the ions[68] or coupled reorganization of the cation and anion[69] have been proposed to explain the solvation dynamics. Shim and Kim have further elaborated the solvation mechanism, which indicates that electrostriction plays a dominant role for solvation of benzene-like species.[70,71] The time scale for the slower decay correlates well with the solvent viscosity.[6,58] It is worth noting that, when the stretched exponential model is used to fit the data, the exponent β is generally about 0.5, indicating highly nonexponential kinetics, though β varies between 0.3−0.9 for different ILs and temperatures.[9,58,61] However, the existence of a shorter time process is indicated by the shift of the earliest observed emission spectrum from the position of the estimated time-zero spectrum.[72] The earliest phase of solvation has often not been fully resolved, because time-correlated single-photon counting (TCSPC) instrument response times are of the order of tens of picoseconds. However, fluorescence upconversion, stimulated emission, and Kerr-gated emission spectroscopy have been employed recently to investigate this process on subpicosecond timescales.[19,60,61,73] Optical Kerr-effect spectroscopy has also been used to characterize the intermolecular dynamics,[20,37−40,43−47] and the fast time scale response is most often attributed to local librational movements of the imidazolium cation.[20,37,40,43−47]

In contrast to the imidazolium ionic liquids, less is known about the dynamics of ammonium based liquids. The earliest studies of solvation dynamics in molten salts were carried out on tetraalkylammonium perchlorate and hydrogen sulfate salts at elevated temperatures. The solvation in these molten salts was found to occur on two timescales. Both timescales were dependent upon cation size and slower than that observed for molecular liquids.[74−76] More recently, the first solvation dynamics study was carried out on an ammonium room-temperature ionic liquid, N_{1444}^+/NTf_2^-.[58] In contrast to the imidazolium ionic liquids, most of the fluorescence red-shifted for this ionic liquid was resolved, and it was concluded that there is little or no rapid relaxation component. The fast solvation component was also not observed in phosphonium-based ionic liquids.[12,58] The solvation response observed for these liquids was highly nonexponential and was fit to Kohlrausch functions. It is of note that the long time scale solvent reorganization dynamics observed for each of the phosphonium ionic liquids, while tracking with liquid viscosity, occurs over a time scale that is a factor of 5 slower than that observed for the imidazolium, ammonium, and pyrrolidinium classes of ionic liquids.[12] The relaxation response of the only pyrrolidinium ionic liquid previously reported using the TDFSS technique was found to be similar to that observed for the class of ILs with imidazolium cations. The response contained a rapid component followed by a slower decay that was fitted to a double exponential.[14]

Two of the four ILs discussed in this paper have been previously investigated using nonlinear optical spectroscopy. The ultrafast dynamics for a family of pyrrolidinium ionic liquids containing different anion/cation combinations were recently investigated using femtosecond optical-heterodyne-detected Kerr effect spectroscopy.[39] The observed picosecond relaxation processes were highly nonexponential and were analyzed using a triexponential model with fast and intermediate relaxation time constants of about 2 and 20 ps for each of the liquids investigated. The longest relaxation time constant was found to correlate with the product of the shear viscosity and the sum of anion and cation volumes and so is roughly consistent with the Stokes−Einstein−Debye (SED) hydrodynamic model for orientational friction.[39] We note that Fayer and co-workers have successfully described the Kerr relaxation dynamics of ethylmethylimidazolium nitrate and tosylate, and *N*-propyl-3-methylpyridinium NTf_2^- ILs using models from mode coupling theories having power law relaxations on intermediate timescales.[10,20]

Time-resolved fluorescence anisotropy measurements have been employed to probe the local rotational friction experienced by a fluorescent molecule following excitation. Although these experiments are also essential to the understanding of the overall dynamics of solvents, to date, less data of this type has been reported for ionic liquids.[9,12,59] If hydrodynamic theory holds

for this new class of solvents, the rotation time constants should be proportional to viscosity and inversely proportional to temperature. The rotational friction experienced by the fluorescent probe 4-aminophthalimide in the imidazolium ionic liquid butylmethylimidazolium hexafluorophosphate can be described by a single exponential anisotropy decay, and is found to conform to predictions made from hydrodynamic theory.[9] Recent experiments on ammonium NTf_2^- salts[77] and phosphonium salts of several anions[12] indicate that rotational anisotropy decay occurs over a broad distribution of relaxation times allowing comparisons to be drawn between ionic liquids and glass-forming organic solvents.[12]

The thermal properties of the four ionic liquids N_{1444}^+/NTf_2, N_{6444}^+/NTf_2^-, $Pyrr_{14}^+/NTf_2^-$, and $Pyrr_{1(2O2)}^+/NTf_2^-$ have been characterized by differential scanning calorimetry (DSC) experiments. Glass transition temperatures were obtained for all four ILs. Temperature-dependent viscosities were measured for each of the ILs, and the Vogel−Tammann−Fulcher function was used to analyze the data. Time-resolved TDFSS and fluorescence anisotropy measurements were carried out for six temperatures from 278.2 to 353.2 K. For the two ammonium-cation ILs N_{1444}^+/NTf_2^- and N_{6444}^+/NTf_2^-, this range of temperatures included observations in the supercooled regime below the melting point. For most of the observed sample temperatures, both the TDFSS and the polarization anisotropy dynamics required at least three exponential functions to adequately fit the spectral time correlation functions.

Experimental Methods

Preparation and Purification of the Ionic Liquids. Pyrrolidinium bromide salts were synthesized via reaction of *N*-methylpyrrolidine with a slight excess of 1-bromobutane or 2-bromoethyl-ethyl ether in acetonitrile for 24 h at 323 K under an inert atmosphere, followed removal of the solvent by rotary evaporation. The resulting solid $Pyrr_{14}^+/Br^-$ or liquid $Pyrr_{1(2O2)}^+/Br^-$ was washed with ethyl acetate, redissolved in acetonitrile and stirred with activated charcoal overnight then passed three times through activated alumina columns. Conversion of the bromides to bis(trifluoromethylsulfonyl)imide salts was performed using equimolar quantities of the bromide salt and $Li^+NTf_2^-$ in aqueous solution. The aqueous layer was removed and the liquid was washed with aliquots of water until no bromide was detectable in the washings (silver acetate test). The pyrrolidinium NTf_2^- ionic liquids were further purified by stirring with activated charcoal overnight then passing through an activated alumina column. All ionic liquids were dried at reduced pressure at 318 K for at least 24 h prior to characterization. N_{1444}^+/NTf_2^- and N_{6444}^+/NTf_2^- were kindly provided by Dr. Pedatsur Neta of NIST, and prepared as described by Skrzypczak and Neta.[78,79]

Differential Scanning Calorimetry. DSC measurements were made on 5−15 mg samples in hermetically sealed aluminum pans using a TA Instruments Q100 differential scanning calorimeter fitted with the LNCS liquid nitrogen cooling system. The temperature scan rate was 10 K/min for all of the measurements reported here.

Viscosity Measurements. A Cambridge Applied Systems (now Cambridge Viscosity) ViscoLab 4100 automated viscometer, equipped with a flow-through temperature control jacket, was used for all viscosity measurements. A Lauda Brinkmann RMT-6 recirculating chiller provided temperature control of ±0.1 K. Each of the ionic liquids was equilibrated at each temperature for at least 20 min prior to the start of the viscosity measurements. Calibrated stainless steel pistons of varying diameters were used to measure viscosities in the range from 1 to 10^4 cP. The viscometer head was placed inside a plastic bag that was continuously purged with nitrogen for the duration of the measurements in order to avoid absorption of moisture from the air by the sample. The viscosities were measured over a temperature range from about 283 to 353 K for N_{6444}^+/NTf_2^- and $Pyrr_{1(2O2)}^+/NTf_2^-$, and from 283 to 363 K for N_{1444}^+/NTf_2^- and $Pyrr_{14}^+/NTf_2^-$.

Preparation of the C153 Ionic Liquid Samples. Coumarin 153 (C153) from Acros Organics was used as received for each of the samples. For preparation of the C153 solutions in the three ILs N_{1444}^+/NTf_2^-, N_{6444}^+/NTf_2^-, and $Pyrr_{1(2O2)}^+/NTf_2^-$, a small volume of concentrated methanol solution of C153 was prepared, and 20−100 μL was added to a small volume of the IL. Additional neat IL was added to achieve an absorbance value of about 0.10 at 420 nm. The methanol was removed under vacuum before further spectroscopic characterization of the sample. The C153 $Pyrr_{14}^+/NTf_2^-$ sample was prepared by addition of solid C153 to the IL, followed by dilution with neat IL until a suitable value of absorbance (typically 0.10) was achieved at 420 nm. Baseline-corrected absorption spectra were measured using a Cary-Varian model 50 spectrophotometer that has a fixed 1.5 nm optical bandpass. Each of our C153 ionic liquid solutions was dried at 313 K under vacuum (≈0.01 Torr) for 24 h prior to spectroscopy experiments. Because several experiments required 8−10 h or more of instrument time at ambient conditions, for between 2 and 5 days, samples may have absorbed atmospheric moisture. Samples were placed in a desiccator overnight between spectroscopy experiments. We mimicked the treatment given our samples that were prepared for sequential measurements of the time-dependent fluorescence Stokes shift and fluorescence anisotropy for six discrete temperatures, which usually took 5 days of data acquisition time. To reproduce the conditions of our experimental fluorescence samples under the worst case, we prepared the samples using the 24-h vacuum oven method, waited 5 days, and then measured the water content by Karl Fischer titration using a Mettler-Toledo DL39 Coulometric titrator. Several determinations of water content were made for each sample; the average and standard deviation values are reported. The water content (in units of ppm by mass) for the IL samples was as follows: N_{1444}^+/NTf_2^-, 227 ± 25 ppm; N_{6444}^+/NTf_2^-, 409 ± 67 ppm; $Pyrr_{14}^+/NTf_2^-$, 496 ± 21 ppm; and $Pyrr_{1(2O2)}^+/NTf_2^-$, 220 ± 8 ppm.

Steady-State Excitation and Emission Spectroscopy. Sample cuvettes were 5 × 10 mm fused silica from NSG Precision Cells with four polished windows. Absorption spectra were measured with a geometry having a 5 mm optical path, whereas all steady-state and time-resolved emission spectra were measured with a 10 mm optical path for excitation.

Steady-state fluorescence emission and excitation spectra of C153 in each of the four ionic liquids were measured with a Spex Fluoromax-3 fluorometer using 420 nm excitation and 520 nm emission wavelengths. Calcite polarizers were used in the fluorometer for steady state anisotropy measurements. The sample temperature was controlled to ± 0.1 K using a Wavelength Electronics thermoelectric temperature controller. Sample equilibration time at each temperature was 10 min. The slits on the Fluoromax-3 instrument were set for 1.0 nm optical bandpass for both the excitation and emission monochromators. The Spex Fluromax-3 wavelength scales for the excitation and emission monochromators are accurate to better than 0.5 nm, because we have an internal consistency check for observation of the scattered excitation, solvent Raman scattering, and second-order diffraction of the scattered excitation from the emission

grating, which are all observed at the relevant wavelength values. However, we are using the internal correction for the emission spectrum provided by the manufacturer and set in the instrument firmware without further calibration.

Time-Resolved Fluorescence. The time-resolved emission data for both the TDFSS solvation and reorientational dynamics for the C153 probe in the four ILs were acquired using the time-correlated single-photon counting (TCSPC) method on a laboratory-built instrument. The TCSPC setup has been described in detail recently,[80−86] so only a brief description is given here. The multichannel analyzer in the Becker and Hickl SPC-630 instrument collected 4096 channels for each fluorescence transient, with a full time window of 70 ns. The instrument response width used here is typically 70 ps fwhm. We have found that it is essential to use a 70 ns acquisition time window for C153 in ILs in order to fully capture the long time dynamics, especially for the case of the fluorescence anisotropy experiment, so that the transient intensity decays completely to the baseline for each of the three polarization transients.

The frequency-doubled laser excitation wavelength for C153 was 420 nm. Fluorescence transients for TDFSS analysis were measured at the magic angle (VM polarization) to eliminate rotational contributions to the transients. A quartz depolarizing optic is placed in front of the spectrometer entrance slit to eliminate the grating polarization bias of the detected fluorescence signal. TDFSS transients were collected typically for 14 wavelengths, corresponding to frequencies spanning the range from 22 750 to 16 250 cm^{-1} in increments of 500 cm^{-1}. Each transient was fit to a multiexponential model with between two to five exponential components using a nonlinear least-squares convolute-and-compare algorithm written in Igor Pro macros.[87]

C153 reorientational dynamics were obtained by measuring the fluorescence anisotropy using three polarization conditions. Vertically polarized excitation was used with the emission detected at polarization angles parallel (VV), perpendicular (VH), and at the magic angle (VM) with respect to the vertically polarized excitation. The C153 excitation wavelength was also 420 nm. An emission frequency of 19 250 cm^{-1} (519.5 nm) was chosen to minimize the short- and long-time perturbations to the transient that arise from the TDFSS effect. To obtain fluorescence anisotropy results with any accuracy for reorientational time constants that are longer than the fluorescence lifetime, substantial care must be taken both during the experiments and the analysis. Any small systematic error in the "G-factor"[54,55,88] that is normally used to account for any differences in the data acquisition between the VV and VH channels will lead to rather dramatic changes in the longer time-scale anisotropy function. In the worst case, a tail-matching data analysis procedure can actually subtract out significant long-time dynamics from the anisotropy. Realizing these potential pitfalls, we used an analysis procedure for the fluorescence anisotropy that does not use tail-matching, but rather does a simultaneous fit of the VV, VM, and VH transients[82,86] using the Igor FitAllAtOnce function.[87] This is a modification of the procedure introduced by Cross and Fleming in 1984[88] with the addition of including the VM transient in the simultaneous fitting analysis. In lieu of a fixed G-factor, each of the VV, VM, and VH intensities is multiplied by an arbitrary scale factor during the fit, which is then used to determine how close the experimental G-factor would be to the ideal value of unity. The relevant equations[54,55] are given below as eqs 1−5.

$$K(t) = \sum_{i=1}^{n} \alpha_i \exp\left(\frac{-t}{\tau_i}\right) \tag{1}$$

$$I_{VM}(t) = K(t) \tag{2}$$

$$I_{VV}(t) = \frac{1}{3} K(t)(1 + 2r(t)) \tag{3}$$

$$I_{VH}(t) = \frac{1}{3} K(t)(1 - r(t)) \tag{4}$$

$$r(t) = \sum_{j=1}^{n} r_i \exp\left(\frac{-t}{\tau_{j,\mathrm{rot}}}\right) \tag{5}$$

To validate our procedures for the numerical analysis and fitting of the TCSPC data, we convolute our fit model parameters with the measured instrument response, add simulated noise according to Poisson statistics, and analyze the simulated data.[81] Previous experience gives us confidence that we can easily resolve five unique exponential time constants for the VM polarization data used in both the TDFSS and anisotropy experiments.[85,86] For fluorescence anisotropy analysis, we can confidently discriminate between two- and three-exponential anisotropy models, but we cannot always differentiate between three- and four-exponential anisotropy models. Because the TCSPC data are measured over a 70 ns time window, we have fully captured all of the baseline, rise, and decay parameters and truncated any nonlinear regions at the start and end of the transients (arising from nonlinearities inherent in any analog electronic time-to-amplitude converter).[89] Using this level of care in the data collection enables us to confidently extract reorientational dynamics with time constants to 100 ns with about a 5% estimated uncertainty and to 200 ns with a 30% estimated uncertainty. For anisotropy time constants beyond about 250 ns, we have reduced confidence in the numerical accuracy of the fits. However, we do have confidence that long values of the anisotropy time constants obtained from the numerical fitting do predict the existence of slowly reorienting species.

Results and Discussion

Phase Behavior−DSC Results. DSC scans were recorded for each of the ionic liquids used in this study. The traces are shown in Figure 2 and the results are presented in Table 1. Our results for N_{6444}^+/NTf_2^- and $Pyrr_{14}^+/NTf_2^-$ are consistent with previous reports.[31,90] Like the related IL N_{6444}^+/NTf_2^-, the methyl derivative N_{1444}^+/NTf_2^- melts slightly above room temperature at 300 K. Thus, the TDFSS relaxation measurements at 278.2 and 293.2 K in those liquids were performed on supercooled solutions. DSC scans of the tetraalkylammonium salts recorded in the cooling direction did not show a freezing transition. However, on the upward scans, cold crystallization occurred in both cases with onset temperatures of about 243 K, as compared to 215 K for $Pyrr_{14}^+/NTf_2^-$. According to the VTF viscosity fitting described in the next section, the viscosities at the cold crystallization onset temperature were approximately 730 000 cP for the ammonium salts and 650 000 cP for $Pyrr_{14}^+/NTf_2^-$. The cold crystallization exotherms for the ammonium ions are significantly broader than that for the pyrrolidinium ion. Enthalpies of fusion (ΔH_f) for N_{1444}^+/NTf_2^-, N_{6444}^+/NTf_2^-, and $Pyrr_{14}^+/NTf_2^-$ were 14.8, 16.3, and 10.7 J/mol, respectively. Since $\Delta G_f = 0$ at T_m, ΔS_f may be calculated from the relationship $\Delta S_f = \Delta H_f/T_m$, and our result of 42 J/mol·K agrees with the 41 J/mol·K value obtained by MacFarlane, et al.[90] $Pyrr_{1(2O2)}^+/NTf_2^-$ showed no melting transition but instead showed a small but reproducible negative change in heat capacity at 235 K. N_{1444}^+/NTf_2^- also resembles $Pyrr_{14}^+/NTf_2^-$

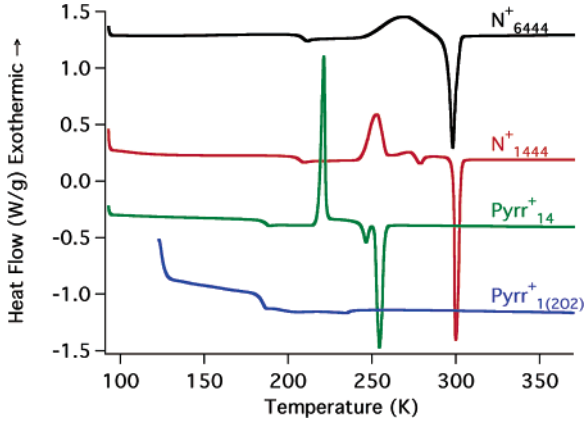

Figure 2. Differential scanning calorimetry traces for the four NTf_2^- ionic liquids, labeled by cation. All scans were recorded at 10 K/min and the signals are offset vertically for clarity (N_{6444}^+: +1.4 W/g, N_{1444}^+: +0.5 W/g, $Pyrr_{14}^+$: −0.2 W/g, $Pyrr_{1(2O2)}^+$: −0.5 W/g). The $Pyrr_{1(2O2)}^+/NTf_2^-$ signal was multiplied by a factor of 2.

TABLE 1: Calorimetric and Viscosity Data for the Four NTf_2^- Ionic Liquids[a]

cation	T_g[b]	$T_{II\to I}$	T_m	ΔH_f	η	$\ln(\eta_0)$	D	T_c	χ^2
N_{1444}^+	205	278[c]	300	14.8	787	−4.12	8.45	164.4	0.0078
N_{6444}^+	206		298	16.3	909	−3.51	7.93	165.8	0.0049
$Pyrr_{14}^+$	184	245[c]	255	10.7	95	−2.28	6.11	154.8	0.0010
$Pyrr_{1(2O2)}^+$	182	235[d]			66	−2.09	5.59	155.1	0.0003

[a] Temperatures are reported in K, ΔH_f in kJ/mol, and viscosities are reported for 293.2 K in units of cP. χ^2 is the value from the nonlinear least-squares fit of the viscosity data to the VTF model. [b] Onset temperatures. [c] Transition between two solid phases. [d] Small decrease in heat capacity.

in that it has an endothermic transition between two solid phases ($T_{II\to I}$), whereas this transition is not observed in N_{6444}^+/NTf_2^-, perhaps due to the breadth of the cold crystallization exotherm.

Dependence of Viscosities on Temperature. The experimental viscosities for the four liquids, measured over a range of temperatures between 283 and 353−363 K, are shown in Figure 3, along with curves representing fits to the logarithmic form of the Vogel−Tammann−Fulcher (VTF) equation:

$$\ln\eta(T) = \ln\eta_0 + \frac{DT_c}{T - T_c} \qquad (6)$$

where $\eta(T)$ is the shear viscosity at temperature T, η_0 is a reference viscosity at which the exponential term is 0, D is the fragility parameter, and T_c is a characteristic temperature for which η diverges. Following the practice of Angell and co-workers,[91] an additional data point with viscosity 10^{13} cP at the glass transition temperature T_g was included in each data set for fitting. The logarithmic VTF equation was fit to the natural log of viscosity to ensure proper fitting over the entire viscosity range; if the exponential form of the VTF equation is fit to actual viscosity, the result often does not account well for the lower viscosity data because of the small absolute magnitude of the errors in that range.

The ammonium and pyrrolidinium ionic liquids group tightly together by family in terms of their VTF fitting parameters. N_{1444}^+/NTf_2^- is slightly less viscous than N_{6444}^+/NTf_2^-, but they have similar D and T_c parameters. The viscosities of the pyrrolidinium salts are about a factor of 10 lower, and the presence of the ether group in $Pyrr_{1(2O2)}^+/NTf_2^-$ results in a decrease in viscosity relative to $Pyrr_{14}^+/NTf_2^-$. The alkyl chain length difference between the two pyrrolidinium salts is not

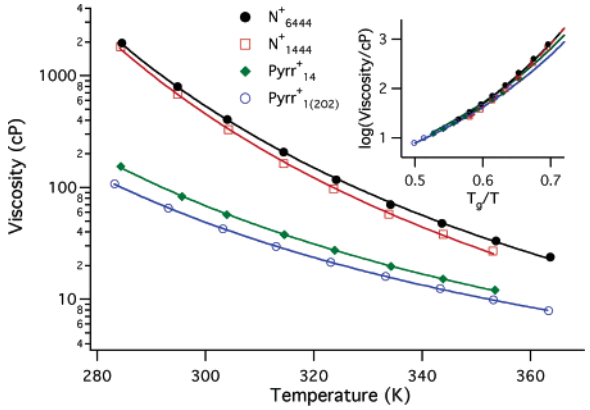

Figure 3. Semilog plot of viscosities versus temperature for the four NTf_2^- ionic liquids, labeled by cation. The measured data points are shown as symbols, and the solid lines are fits to the VTF equation. Inset: Glass transition temperature (T_g) scaled Arrhenius plot of the viscosities and curves calculated from the VTF fits.

significant; the viscosity of the methoxyethyl derivative $Pyrr_{1(2O1)}^+/NTf_2^-$ reported earlier[77] is virtually the same as that of $Pyrr_{1(2O2)}^+/NTf_2^-$ at all temperatures.

Angell and co-workers[91] have used glass transition temperature-scaled Arrhenius plots to characterize the fragility, or the rate at which transport properties change as the glass transition temperature is approached. Fragile liquids show a larger change in properties near T_g, with the rate of change decreasing as the temperature increases, whereas strong ones show linear Arrhenius behavior at all temperatures. Fragility is exemplified by VTF behavior, and the VTF parameters D and T_c can be used to quantify the fragility,[92,93] but that is beyond the scope of the present work. The fragility of the four liquids in question can be evaluated graphically in the T_g-scaled Arrhenius plot inset within Figure 3, which shows them to be very similar, although the fragility of the ammonium salts is slightly smaller as indicated by the higher tangents of the fitted curves on the right side of the inset figure. All four liquids fall close to the location of *N*-butyl-*N*′-methylimidazolium tetrafluoroborate in the viscosity vs T_g/T plot in Figure 6 of ref 91 and fall within the center of the range displayed by other ionic liquids.

Steady-State Fluorescence Spectroscopy. The electronic structure of the C153 fluorescence probe molecule has been widely characterized, in addition to the experimental studies. Several theoretical electronic structure methods have been applied.[94−97] In the most recent work, Ingrosso and co-workers combined the use of quantum methods with solvent models, followed by the use of molecular dynamics simulations in which the charge distributions from the ground- and excited-state quantum results were used with classical potentials for the solvent.[96,97]

Samanta and co-workers have shown that neat ILs may display non-negligible fluorescence intensities.[98,99] Fluorescence probe studies of ILs with nonaromatic cations are simplified relative to studies with aromatic cations (such as imidazoliums or pyridiniums) because background fluorescence from the neat liquid is greatly reduced. Steady-state emission spectra of C153 in each of the four ILs were measured at six temperatures, and the emission maxima at each temperature are presented in Table 2. Representative steady-state fluorescence spectra are presented in the Supporting Information. Empirically speaking, the emission spectra maxima shift to the red with increasing temperature, particularly in the cases of the tetraalkylammonium liquids. In fact, the apparent spectral shift is due to the solvation response times being large fractions of the total emission lifetime, as is

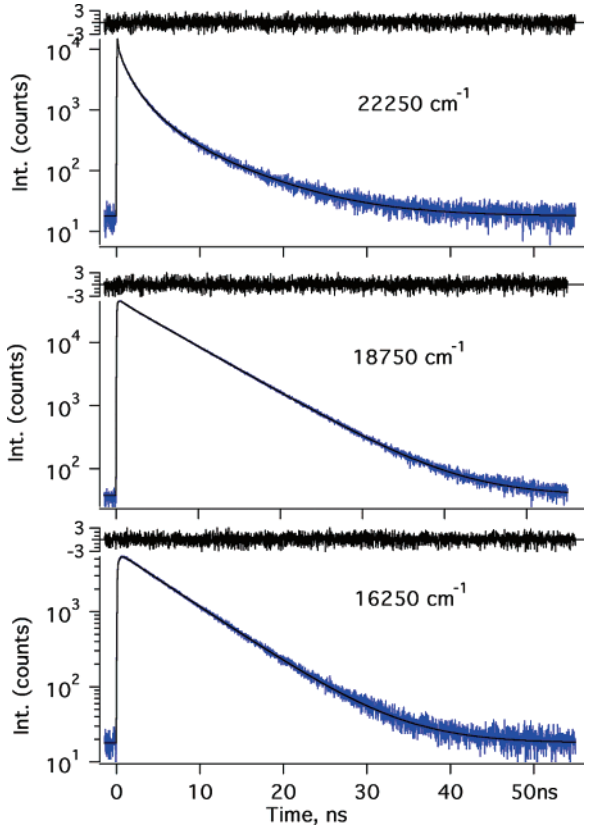

Figure 4. TCSPC transients for C153 in $Pyrr_{14}^{+}/NTf_2^{-}$ at 308.2 K, using 420 nm laser excitation. Three of the 13 frequency-dependent transients are shown, for the bluest wavelength transient at 449.4 nm (top, 22,250 cm^{-1}); for the intermediate wavelength of 533.3 nm (middle, 18 750 cm^{-1}); and for the reddest wavelength transient recorded at 615.4 nm (bottom, 16 250 cm^{-1}). The TCSPC data are shown in blue, with the best fits to 5-exponential (top, bottom) and 4-exponential (middle) models and reduced residuals shown in black. Note that the emission transient for 22 250 cm^{-1} is clearly non-exponential over the entire transient.

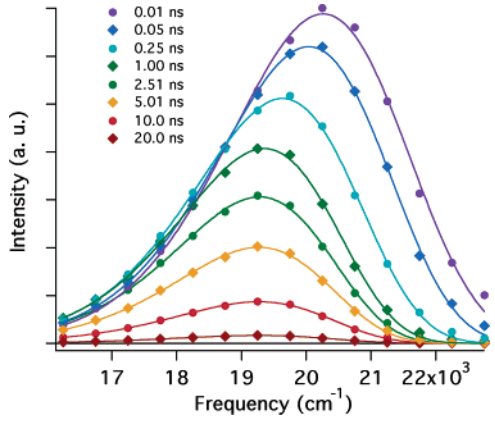

Figure 5. Typical reconstructed emission spectra for C153 in N_{1444}^{+}/NTf_2^{-} at 338.2 K. The circles represent the intensity of the emission at the given time slice, while the solid lines are the log-normal fits to the transient spectra. From top to bottom, the spectra are plotted for time slices at 0.01, 0.05, 0.251, 1.0, 2.51, 5.01, 10.0, and 20.0 ns.

shown by the graphs of frequency shift transients in Figure 6 below. As the temperature increases, the solvation response time becomes shorter, resulting in progressively smaller, approaching negligible, contributions of the bluer transient emission spectra at short times to the steady-state emission spectra.

The potential effects of emission from neat ILs with saturated cations was studied for the case of $Pyrr_{14}^{+}/NTf_2^{-}$. Steady-state

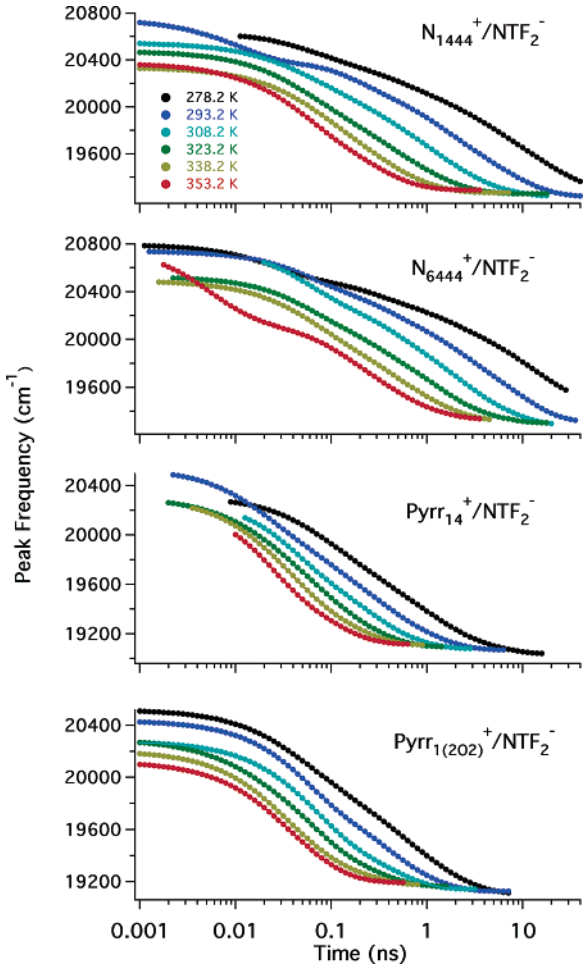

Figure 6. log−log plots of the TDFSS frequency shift transients (from top to bottom): N_{1444}^{+}/NTf_2^{-}, N_{6444}^{+}/NTf_2^{-}, $Pyrr_{14}^{+}/NTf_2^{-}$, and $Pyrr_{1(202)}^{+}/NTf_2^{-}$.

TABLE 2: C153 Emission Maxima and Estimated Values of π^* from C153 Fluorescence for the Four NTf_2^{-} ILs as a Function of Temperature[a]

	N_{1444}^{+}		N_{6444}^{+}		$Pyrr_{14}^{+}$		$Pyrr_{1(202)}^{+}$	
T	$\nu_{em,max}$	est. π^*	$\nu_{em,max}$	est. π^*	$\nu_{em,max}$	est. π^*	$\nu_{em,max}$	est. π^*
278.2	19872	0.384	20028	0.339	19265	0.557	19280	0.553
293.2	19637	0.451	19802	0.404	19207	0.574	19249	0.561
308.2	19468	0.499	19620	0.456	19187	0.579	19240	0.564
323.2	19411	0.515	19508	0.487	19186	0.580	19237	0.565
338.2	19376	0.525	19461	0.501	19189	0.579	19247	0.562
353.2	19371	0.527	19439	0.507	19203	0.574	19252	0.561

[a] Frequency units are cm^{-1}, and temperatures are in K.

fluorimetry showed that the background emission from neat $Pyrr_{14}^{+}/NTf_2^{-}$ was featureless and accounted for less than 1.4% of the emission at 530 nm from C153 at the coumarin concentration used for these measurements. TCSPC transients showed a ≈2.4 ns lifetime for decay of very weak emission at 530 nm, with a temporal emission maximum corresponding to 0.3% of the maximum emission measured for the sample of $Pyrr_{14}^{+}/NTf_2^{-}$ with C153. Thus, no long lifetime dynamics can be ascribed to the emission from the neat $Pyrr_{14}^{+}/NTf_2^{-}$, and we believe the same will be true for each of the four nonaromatic cation ILs discussed here.

Using a relation obtained for a series of polar aprotic solvents, Horng et al.[53] developed a correlation between the steady-state emission spectra of C153 and the standard empirical solvent polarity scale π^*. The relationship between π^* and the C153

TABLE 3: Fit Parameters for the C153 Time-Dependent Emission Shift in the Ionic Liquid N_{1444}^+/NTf_2^- [a]

T	$\nu_{em}(t\rightarrow\infty)$	A_1	τ_1	A_2	τ_2	A_3	τ_3	A_4	τ_4	t_{start}	t_{end}	τ_0	$\tau_{1/e}$	$\langle\tau\rangle$
278.2	19276	228	0.0648	243	0.527	358	4.12	544	21.7	0.011	70.8	0.336	5.90	9.79
293.2	19239	324	0.0093	254	0.217	425	1.46	513	7.65	0.001	44.7	0.0417	1.68	3.04
308.2	19239	278	0.0441	269	0.240	475	1.16	286	4.13	0.001	17.8	0.166	0.826	1.38
323.2	19260	366	0.0457	240	0.195	301	0.532	309	1.48	0.001	17.8	0.122	0.348	0.560
338.2	19269			336	0.0582	404	0.224	328	0.703	0.001	7.10	0.133	0.229	0.319
353.2	19291	15	0.00677	476	0.0464	384	0.204	208	0.466	0.001	3.55	0.0734	0.127	0.183

[a] Frequencies and amplitudes A_i are reported in units of cm^{-1}, temperatures in K, and time constants τ_i and fit points t_{start} and t_{end} in ns.

TABLE 4: Fit Parameters for the C153 Time-Dependent Emission Shift in the Ionic Liquid N_{6444}^+/NTf_2^- [a]

T	$\nu_{em}(t\rightarrow\infty)$	A_1	τ_1	A_2	τ_2	A_3	τ_3	A_4	τ_4	t_{start}	t_{end}	τ_0	$\tau_{1/e}$	$\langle\tau\rangle$
278.2	19494	255	0.0245	174	0.262	211	1.51	664	13.6	0.011	28.2	0.116	3.70	7.21
293.2	19311	266	0.0577	213	0.338	333	1.72	621	9.26	0.0126	35.5	0.260	2.73	4.47
308.2	19284	412	0.0490	265	0.337	447	1.57	399	5.74	0.020	20.0	0.160	1.38	2.04
323.2	19299	311	0.0542	232	0.252	488	1.13	208	3.97	0.00236	17.8	0.174	0.768	1.17
338.2	19322			380	0.0558	363	0.306	429	1.21	0.00158	4.47	0.140	0.365	0.554
353.2	19330	604	0.00545	247	0.112	383	0.329	236	1.01	0.00177	3.55	0.0128	0.170	0.270

[a] Frequencies and amplitudes A_i are reported in units of cm^{-1}, temperatures in K, and time constants τ_i and fit points t_{start} and t_{end} in ns.

TABLE 5: Fit Parameters for the C153 Time-Dependent Emission Shift in the Ionic Liquid $Pyrr_{14}^+/NTf_2^-$ [a]

T	$\nu_{em}(t\rightarrow\infty)$	A_1	τ_1	A_2	τ_2	A_3	τ_3	A_4	τ_4	t_{start}	t_{end}	τ_0	$\tau_{1/e}$	$\langle\tau\rangle$
278.2	19034	382	0.0786	256	0.290	438	1.07	214	4.19	0.00891	15.9	0.208	0.630	1.140
293.2	19068	422	0.0179	278	0.0722	414	0.263	369	1.02	0.00224	6.31	0.0506	0.194	0.346
308.2	19077			539	0.0364	453	0.199	264	0.588	0.0126	2.82	0.0716	0.173	0.211
323.2	19091	216	0.0174	454	0.0519	356	0.160	189	0.351	0.002	1.41	0.0508	0.0891	0.124
338.2	19107			256	0.0201	540	0.0407	410	0.168	0.00355	0.891	0.0424	0.0631	0.0796
353.2	19116					729	0.0209	484	0.103	0.010	0.631	0.0306	0.0562	0.0535

[a] Frequencies and amplitudes A_i are reported in units of cm^{-1}, temperatures in K, and time constants τ_i and fit points t_{start} and t_{end} in ns.

TABLE 6: Fit Parameters for the C153 Time-Dependent Emission Shift in the Ionic Liquid $Pyrr_{1(2O2)}^+/NTf_2^-$ [a]

T	$\nu_{em}(t\rightarrow\infty)$	A_1	τ_1	A_2	τ_2	A_3	τ_3	A_4	τ_4	t_{start}	t_{end}	τ_0	$\tau_{1/e}$	$\langle\tau\rangle$
278.2	19109	323	0.0363	229	0.0953	411	0.441	448	1.68	0.001	7.10	0.113	0.409	0.686
293.2	19125			608	0.0524	452	0.366	254	0.995	0.001	7.10	0.100	0.201	0.342
308.2	19144					694	0.0619	440	0.406	0.001	3.16	0.0921	0.126	0.195
323.2	19163			146	0.00974	636	0.0538	350	0.263	0.001	1.58	0.040	0.0790	0.113
338.2	19174			419	0.0254	341	0.0496	273	0.186	0.001	0.794	0.0416	0.0524	0.0757
353.2	19194					459	0.0257	469	0.0765	0.001	0.562	0.0387	0.0463	0.0514

[a] Frequencies and amplitudes A_i are reported in units of cm^{-1}, temperatures in K, and time constants τ_i and fit points t_{start} and t_{end} in ns.

emission maximum is given by $\nu_{em}[cm^{-1}] = 21\,217 - 3505{\cdot}\pi^*$. The values of π^* obtained using this formula are summarized in Table 2 for all liquids and temperatures. Clearly, the estimated π^* values obtained from partially unrelaxed emission spectra at lower temperatures (less than 338 K for the ammonium salts and less than 293 K for the pyrrolidinium salts) are not representative of the actual steady-state polarities of the liquids. They are presented to demonstrate the need to take the solvation dynamics into account when using spectroscopic measurements to estimate ionic liquid properties. The π^* values at 353 K can be reasonably taken to indicate the relative polarity of the ionic liquids, with the pyrrolidinium salts being slightly more polar than the ammonium ones. This is consistent with E_T^N values measured for N_{1444}^+/NTf_2^- (0.494), $Pyrr_{14}^+/NTf_2^-$ (0.552), and $Pyrr_{1(2O2)}^+/NTf_2^-$ (0.552) using betaine-30 dye. The estimated polarities are similar to estimates obtained by others for ionic liquids with both aromatic and nonaromatic cations.[7,11,14,100,101]

Time-Resolved Fluorescence Spectroscopy Using TCSPC. *1. Solvation Dynamics for the Four ILs from C153 TDFSS Data.* Figure 4 shows typical graphs of TCSPC transients for the highest, middle, and lowest frequencies of C153 fluorescence that were measured for reconstruction of the time-dependent emission spectra. In Figure 4 (top), the transient for C153 in N_{1444}^+/NTf_2^- at 298.2 K measured at 22 250 cm^{-1} emission frequency is shown; the transient at 17 850 cm^{-1} is shown in Figure 4 (middle), and the transient for 16 250 cm^{-1} emission is shown in Figure 4 (bottom). The data are fit to a sums-of-exponentials model using a convolute-and-compare nonlinear least-squares analysis. The reduced residuals from the fitting procedures are shown above the curves. Generally, a five-exponential model is required to obtain an adequate fit to the emission transients for either the highest or lowest frequencies.

Because our true goal in the TDFSS experiments is to obtain the frequency shift of the time-dependent emission spectra, we do not assign any of the five exponential time constants to specific molecular dynamical processes, but we use the fits to calculate spectra at a range of delay times. We use the standard spectral reconstruction method for TDFSS data.[52,53,102,103]

A typical C153 time-dependent emission spectrum reconstructed from the 13 TDFSS transients is shown in Figure 5 for the ionic liquid N_{1444}^+/NTf_2^-. The data points are shown as closed circles, with the log-normal spectral fit function shown as the solid line. Because the TDFSS dynamics are quite heterogeneous, we calculate reconstructed spectra for 101 time slices with log-time spacing from 1 ps to 100 ns. The combination of our temporal instrument response and the time increment per channel of 17.1 ps prevents us from resolving the IL solvation dynamics below about 10 ps. For this reason, we choose to report the emission frequency time-correlation function $\tilde{\nu}_{em}(t)$ rather than the more widely used normalized solvation function $C(t)$ or $S_\nu(t)$. In this work, $\tilde{\nu}_{em}(t)$ represents the peak frequency resulting from the log-normal fits to the

reconstructed time-dependent emission spectra. The ansatz of Fee and Maroncelli enables a sensible estimation of the early time spectrum by comparison to low-temperature spectra of the solvatochromic probe molecule in a nonpolar solvent.[72] However, simply reporting the non-normalized frequency shift enables a more direct comparison in the future between different experiments performed in different labs with different intrinsic time resolution.

The solvation dynamics frequency-shift function $\tilde{\nu}_{em}(t)$ for C153 in each of our four ILs are shown in Figure 6 for the set of sample temperatures {278.2, 293.2, 308.2, 323.2, 338.2, and 353.2 K}. Each of the frequency-shift functions $\tilde{\nu}_{em}(t)$ has been fit to a number of model functions, including sums of exponentials and a Kohlrausch function. In no case did we obtain an adequate fit to a Kohlrausch function. To achieve good quality fits to the C153 emission shift functions, a sum of two, three, or four exponentials was required, with fewer exponentials needed as the sample temperature for the measurement was increased. The best fits to the temperature-dependent C153 emission shift dynamics in the four ILs are summarized in Tables 3−6. As first shown by Horng, et al., we report the rate-averaged solvation time constant (τ_0), the effective time constant to reach the 1/*e* point of the decay ($\tau_{1/e}$), and the averaged solvation time constant ($\langle\tau\rangle$), which is strongly biased toward the longest time constant.[53]

As has been observed previously by Maroncelli and co-workers, for solvation dynamics in a number of IL systems, there is a strong correlation with these effective solvation time constants and the measured macroscopic shear viscosities of the ILs.[9,58] This is reflected by the data in Tables 3−6. Figure 7 plots each of the three effective solvation dynamics time constants τ_0, $\tau_{1/e}$, and $\langle\tau\rangle$ vs the ratio of viscosity to absolute temperature, η/T. The C153 solvation time constants for alkylammonium NTf_2^- ILs roughly scale with the viscosities relative to the pyrrolidinium NTf_2^- ILs, given that the viscosities for the former are about an order of magnitude larger than for the latter.

Both the timescales and qualitative shapes of the C153 frequency-shift functions $\tilde{\nu}_{em}(t)$ for N_{1444}^+/NTf_2^- and N_{6444}^+/NTf_2^- are rather different from those of $Pyrr_{14}^+/NTf_2^-$ and $Pyrr_{1(2O2)}^+/NTf_2^-$, as seen in Figure 6. The $\tilde{\nu}_{em}(t)$ functions for C153 in the dialkylpyrrolidinium ILs show only slight modulations in curvature, whereas the time correlation functions for the tetraalkylammonium liquids show inflection points in the log−log plots of $\tilde{\nu}_{em}(t)$ vs time, thus clearly indicating that these must require a sum of exponential fits, and cannot be properly fit by a stretched-exponential function.

Figure 6 demonstrates that, although we resolve a large fraction of the total solvent relaxation at the lower temperatures, we cannot fully resolve the early time solvation dynamics at higher temperatures. Better time resolution data for TDFSS solvation dynamics can be obtained using fluorescence upconversion or Kerr-gated emission. Primarily because of the required sample volumes for our fluorescence upconversion experiment, and because we can only perform room-temperature upconversion experiments, we have not yet measured the C153 solvation dynamics using our upconversion apparatus. Solvation dynamics in ILs has been characterized with substantially superior time resolution by several groups.[18,19,60,61] Recent work by Lang, Angulo, and Vauthey discussed the C153 TDFSS data for a pair of imidazolium NTf_2^- ionic liquids. Though they have demonstrated time resolution of 230 fs in their fluorescence dynamics, they observed less of the spectral relaxation for C153 emission in their imidazolium ILs than we report here for our tetraalkylammonium and dialkylpyrrolidinium NTf_2^- ILs. A

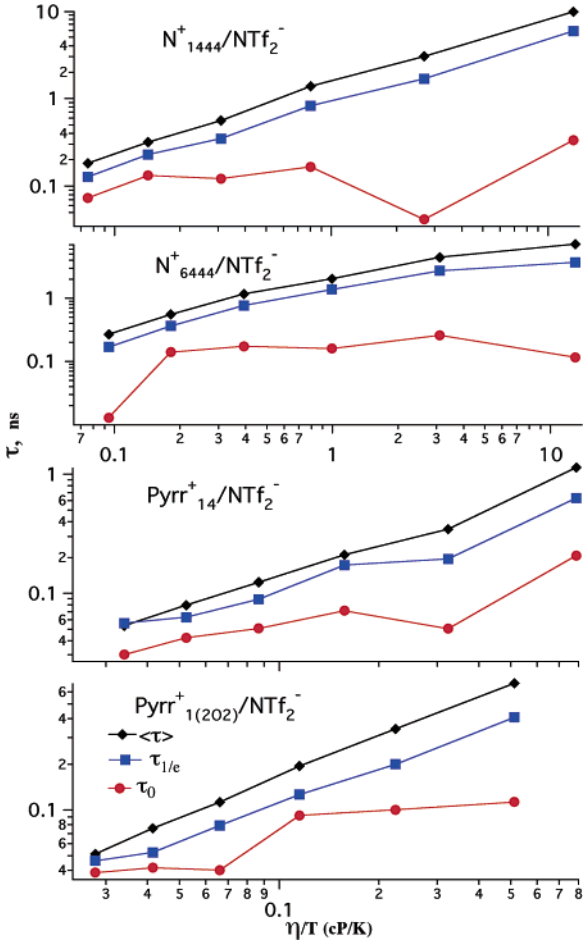

Figure 7. TDFSS time constants (in units of ns) plotted vs the ratio of viscosity over temperature (in units of cP/K) for the ILs (top to bottom): N_{1444}^+/NTf_2^-, N_{6444}^+/NTf_2^-, $Pyrr_{14}^+/NTf_2^-$, and $Pyrr_{1(2O2)}^+/NTf_2^-$. Log−log plots are used to enable visualization of all of the data points; lines are not fits but simply connect the data points. $\langle\tau\rangle$ (black diamonds), $\tau_{1/e}$ (blue squares) and τ_0 (red circles). The graph abscissa ranges from 0.07 to 14.0 cP/K for the top two graphs, and spans 0.025 to 0.8 cP/K for the bottom two graphs.

detailed study comparing the time-resolved spectral shifts obtained using subpicosecond Kerr-gated emission studies with picosecond resolution TCSPC experiments has been conducted by Maroncelli and co-workers. Using the DCS fluorescence probe, they studied five imidazolium ILs and $Pyrr_{13}^+/NTf_2^-$, a pyrrolidinium liquid analogous to our $Pyrr_{14}^+/NTf_2^-$.[73] Clearly biphasic behavior was observed for all liquids, with the fast time scale dynamics attributed to the inertial dynamics of the constituent ions.

A comparison of the temperature dependence of the effective solvation time constants τ_0, $\tau_{1/e}$, and $\langle\tau\rangle$ is given in Table 7 for the four ILs. In all cases, a superior or at least equivalent quality fit is obtained using the log form of the VTF function for the solvation rates, given as

$$\ln\left(\frac{1}{\tau}\right) = \ln(k_0) + \frac{DT_c}{T - T_c} \qquad (7)$$

We note that in the limit as T_c approaches zero (or the high-temperature limit), the VTF equation reduces to the Arrhenius equation. Thus it is clear that the solvation dynamics for N_{6444}^+/NTf_2^- are closest to Arrhenius character, with values of T_c ranging between 26 and 44 K for the effective time constants. Another notable point is that the effective time constants for

TABLE 7: VTF and Arrhenius Parameters Obtained by Fitting the C153 TDFSS Time Constants τ_0, $\tau_{1/e}$, and $\langle\tau\rangle$ vs Temperature[a]

		VTF				Arrhenius		
		ln(k_0)	D	T_c	χ^2	ln(k_0)	E_a/R	χ^2
N_{1444}^+/NTf_2^-	τ_0	24.77	−3.897	102.9	2.21	25.61	−863.9	2.22
	$\tau_{1/e}$	27.70	−4.782	179.7	0.0289	36.80	−4912	0.116
	$\langle\tau\rangle$	29.39	−9.781	146.8	0.0130	37.24	−5195	0.0546
N_{6444}^+/NTf_2^-	τ_0	29.33	−68.76	26.55	3.80	30.01	−2211	3.77
	$\tau_{1/e}$	31.95	−69.25	43.46	0.257	33.81	−4081	0.229
	$\langle\tau\rangle$	32.18	−74.50	43.04	0.131	34.12	−4329	0.111
$Pyrr_{14}^+/NTf_2^-$	τ_0	24.12	−0.05660	269.7	0.280	29.88	−1993	0.582
	$\tau_{1/e}$	25.15	−0.8249	229.8	0.114	32.47	−3062	0.258
	$\langle\tau\rangle$	26.33	−1.902	208.5	0.0343	34.60	−3827	0.145
$Pyrr_{1(2O2)}^+/NTf_2^-$	τ_0	27.42	−11.94	77.73	0.199	28.75	−1655	0.197
	$\tau_{1/e}$	26.55	−2.367	187.9	0.0139	32.20	−2911	0.0557
	$\langle\tau\rangle$	29.31	−11.52	115.8	0.00121	33.35	−3393	0.00887

[a] Units of T_c and E_a/R are in K, and k_0 units are in s^{-1}. χ^2 values from the nonlinear least-squares fits are not normalized.

early time dynamics τ_0 show reduced activation energies E_a relative to the longer time scale dynamics. For the intermediate and longer time constants, the values of E_a are larger for the tetraalkylammonium ILs than for the dialkylpyrrolidinium ILs. The values range from about 10 kcal/mol for N_{1444}^+/NTf_2^-, 8 to 9 kcal/mol for N_{6444}^+/NTf_2^-, and 6−8 kcal/mol for $Pyrr_{14}^+/NTf_2^-$ and $Pyrr_{1(2O2)}^+/NTf_2^-$.

The spectral shift dynamics in Figure 6 show incomplete relaxation of the C153 emission spectrum at 278.2 K for both N_{1444}^+/NTf_2^- and N_{6444}^+/NTf_2^-. This is a result of the natural lifetime of the C153 probe being about 5 ns, which is typical of singlet emitting solvatochromic probes. Ito and Richert have demonstrated convincingly that the emission from quinoxaline, an organic solvatochromic molecule that emits from its triplet state, can be used to probe the slow relaxations occurring in deeply supercooled ILs.[15,104] This illustrates that a single solvatochromic emissive probe cannot be used to probe the dynamics over all relevant timescales, because triplet emissive probes cannot be used easily for monitoring femtosecond dynamics (because of the intersystem crossing induction time) and singlet probes cannot be used much beyond their natural radiative lifetime, typically less than 10 ns. A combination of both singlet and triplet probes is clearly warranted if solvation dynamics over the entire range of relevant timescales is to be observed.

2. C153 Reorientation Dynamics. The graphs in Figure 8 present typical results from our fluorescence anisotropy experiments. Out of the experimental time windows of 70 ns and 4096 data points, we usually fit between 3000 and 3400 points in the TCSPC transients, or a time window of about 50 ns. We have found that it is crucial to record the anisotropy data until the transient fluorescence intensity for each of the three polarization angles has decayed fully to the experimental baseline. Using the simultaneous fitting method described above means that we do not need to be overly concerned with the so-called G-factor in the fluorescence anisotropy,[54,55] which for our experimental conditions typically ranges from 0.98 to 1.02, with worst case data having G values in the range from 0.95 to 1.05. The random distribution of the reduced residuals and $\chi_{red.}^2$ value of 1.067 both demonstrate that this 3-exponential anisotropy fit is of quite good quality.

Summaries of all of the fluorescence anisotropy analysis for C153 in the four ILs N_{1444}^+/NTf_2^-, N_{6444}^+/NTf_2^-, $Pyrr_{14}^+/NTf_2^-$, and $Pyrr_{1(2O2)}^+/NTf_2^-$ are given in Tables 8−11, respectively, for the six temperatures from 278.2 to 353.2 K. Several trends are apparent in these data. The values of the limiting anisotropy $r(0)$ are seen to decrease with increasing temperature, which may indicate the appearance of additional

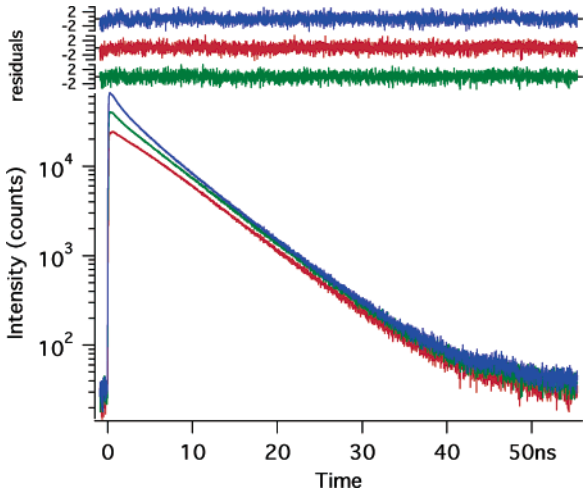

Figure 8. Typical TCSPC fluorescence anisotropy data for C153 in $Pyrr_{1(2O2)}^+/NTf_2^-$ at 293.2 K. The data are color-coded by the combination of emission polarizations measured relative to the vertical excitation polarization at 420 nm. The data are shown in blue for the VV transient, green for the VM transient, and red for the VH transient. The fits to a 3-exponential model for the fluorescence anisotropy are shown as the superposed black line. The corresponding reduced residuals for the simultaneous fit to all three transients are shown at the top, with blue for the VV fit, green for the VM fit, and red for the VH fit.

fast components to the orientational relaxation of C153 that we are not able to resolve with the TCSPC data we have measured. Generally, all of the data can be fit to a three-exponential orientational relaxation equation. Single- and stretched-exponential functions never provided adequate fits to the $r(t)$ orientational relaxation. At the highest temperatures for which we recorded the anisotropies, 353.2 K, a 2-exponential model was adequate to fit the C153 data for the N_{1444}^+/NTf_2^- and $Pyrr_{1(2O2)}^+/NTf_2^-$ liquids. For the ammonium cation ILs, we found that qualitatively the same fits curves result using either two- or three-exponential models for the $r(t)$ function, with the three-exponential model providing a superior fit. More specifically, for N_{1444}^+/NTf_2^- and N_{6444}^+/NTf_2^- the orientational relaxation time constants for a two-exponential model would have values bridging the values of the short and intermediate, and intermediate and long time constants. This was not case for the $Pyrr_{1444}^+/NTf_2^-$ and $Pyrr_{1(2O2)}^+/NTf_2^-$ ILs. For these pyrrolidinium cation ILs, a 2-exponential model provided a not unreasonable fit but again with a superior fit resulting for the 3-exponential model. However, the additional lifetime component recovered was much longer. The values of these longer lifetimes components have non-negligible amplitudes, but

TABLE 8: Time-Dependent Anisotropy Parameters Obtained for N_{1444}^+/NTf_2^- vs Temperature[a]

T	η	$r(0)$	r_1	$\tau_{1,rot}$	r_2	$\tau_{2,rot}$	r_3	$\tau_{3,rot}$	$\tau_{0,rot}$	$\tau_{1/e,rot}$	$\langle\tau\rangle_{rot}$	$\chi_{red.}^2$
278.2	3634	0.395	0.0199	1.02	0.0695	10.3	0.305	242 (256)	14.4	179.5	189	1.039
293.2	786.1	0.382	0.0308	0.623	0.0630	3.71	0.289	46.4 (239)	5.27	33.3	35.7	1.033
308.2	247.1	0.349	0.0564	0.529	0.0741	3.32	0.219	16.5 (284)	2.46	9.35	11.1	1.061
323.2	99.91	0.335	0.0387	0.135	0.0801	0.983	0.216	5.63 (251)	0.825	3.3	3.88	1.069
338.2	48.25	0.383	0.0990	0.0526	0.0797	0.594	0.204	2.74 (265)	0.183	0.95	1.60	1.049
353.2	26.54	0.292			0.0776	0.241	0.214	1.30 (503)	0.599	0.902	1.02	1.071

[a] Temperatures are in K, viscosities η in cP, and time constants $\tau_{i,rot}$ in ns. The numbers in parentheses in the $\tau_{3,rot}$ column are effective molecular volumes in units of A^3 calculated from eq 8. $\chi_{red.}^2$ is the reduced chi-squared value from the nonlinear least-squares fit.

TABLE 9: Time-Dependent Anisotropy Parameters Obtained for N_{6444}^+/NTf_2^- vs Temperature[a]

T	η	$r(0)$	r_1	$\tau_{1,rot}$	r_2	$\tau_{2,rot}$	r_3	$\tau_{3,rot}$	$\tau_{0,rot}$	$\tau_{1/e,rot}$	$\langle\tau\rangle_{rot}$	$\chi_{red.}^2$
278.2	3612	0.363	0.0253	0.692	0.0537	6.76	0.284	132 (140)	7.78	99.6	104	1.072
293.2	909.3	0.375	0.0426	0.513	0.0877	5.52	0.245	63.4 (282)	3.65	36.4	42.7	1.064
308.2	306.2	0.367	0.0528	0.392	0.0887	2.89	0.225	25.0 (347)	2.10	13	16.1	1.075
323.2	126.9	0.346	0.057	0.166	0.0999	1.37	0.189	8.76 (308)	0.787	3.85	5.21	1.061
338.2	61.29	0.334	0.0650	0.117	0.0955	0.838	0.174	3.98 (303)	0.468	1.78	2.3	1.049
353.2	33.27	0.315	0.0778	0.134	0.087	0.724	0.150	2.19 (321)	0.409	1.00	1.27	1.051

[a] Temperatures are in K, viscosities η in cP, and time constants $\tau_{i,rot}$ in ns. The numbers in parentheses in the $\tau_{3,rot}$ column are effective molecular volumes in units of A^3 calculated from eq 8. $\chi_{red.}^2$ is the reduced chi-squared value from the nonlinear least-squares fit.

TABLE 10: Time-Dependent Anisotropy Parameters Obtained for $Pyrr_{14}^+/NTf_2^-$ vs Temperature[a]

T	h	$r(0)$	r_1	$\tau_{1,rot}$	r_2	$\tau_{2,rot}$	r_3	$\tau_{3,rot}$	r_4	$\tau_{4,rot}$	$\tau_{0,rot}$	$\tau_{1/e,rot}$	$\langle\tau\rangle_{rot}$	$\chi_{red.}^2$
278.2	219.1	0.327	0.0141	0.466	0.0502	2.12	0.263	15.5 (271)			4.62	12.1	12.8	1.069
293.2	94.80	0.372			0.0487	0.658	0.266	5.29 (225)	0.0570	220 (9395)	2.98	6.28	37.6	1.066
308.2	48.48	0.333			0.0472	0.358	0.257	2.57 (225)	0.0285	85.5 (7505)	1.43	2.56	9.35	1.043
323.2	28.00	0.323			0.0511	0.325	0.248	1.45 (231)	0.0242	111 (17690)	0.981	1.4	9.46	1.092
338.2	17.72	0.289			0.0279	0.164	0.138	0.647 (171)	0.123	1.11 (293)	0.584	0.75	0.799	1.067
353.2	12.03	0.284			0.0494	0.215	0.219	0.564 (229)	0.0156	1.27 (515)	0.450	0.49	0.542	1.109

[a] Temperatures are in K, viscosities η in cP, and time constants $\tau_{i,rot}$ in ns. The numbers in parentheses in the $\tau_{3,rot}$ and $\tau_{4,rot}$ columns are effective molecular volumes in units of A^3 calculated from eq 8. $\chi_{red.}^2$ is the reduced chi-squared value from the nonlinear least-squares fit.

display a strong covariance with the other anisotropy parameters. Thus, we estimate that the uncertainties in the values of these longer orientational relaxation time constants for $Pyrr_{14}^+/NTf_2^-$ and $Pyrr_{1(2O2)}^+/NTf_2^-$ are quite large, between 50 and 100%.

The C153 fluorescence anisotropy time constants summarized in Tables 8, 9, 10, and 11 show that there is considerable complexity in the reorientation time correlation functions. The value of τ_3 for N_{1444}^+/NTf_2^- at 278.2 K is 242 ns, which has an estimated uncertainty of ±50%. The values for τ_0, $\tau_{1/e}$, and $\langle\tau\rangle$ have uncertainties similar to those discussed above in the Time-Resolved Fluorescence section.

For the pyrrolidinium NTf_2^- liquids, it is also clear that we likely cannot resolve the slowest time constants for C153 reorientation at 278.2 K, the lowest temperature recorded. In Table 10, we use a scheme to represent the anisotropy data for C153 in $Pyrr_{14}^+/NTf_2^-$ in four exponential decay columns, despite the fact that we have resolved only a three exponential model. This is because the time constants obtained for this system the lowest temperature of 278.2 K do not register with those for the higher temperatures. If we consider the temperature dependence of the values of the longest reorientation time constant for $Pyrr_{14}^+/NTf_2^-$, we see that for 293.2 K the value of τ_4 is 220 ns. This means that for the lowest temperature for which we did experiments, we would predict the value of τ_4 to be approaching 1 μs, which is well beyond the range in which we can resolve reorientation values using a probe with an effective 5 ns excited-state lifetime. Thus, we expect that there is a very slow reorientation time constant for $Pyrr_{14}^+/NTf_2^-$ that we are not resolving. This observation for $Pyrr_{14}^+/NTf_2^-$ may give us some insight into the behaviors for the other three liquids. Considering the slowest reorientation time constants τ_3 for $Pyrr_{1(2O2)}^+/NTf_2^-$ in Table 11, we find that the values are scattered widely and, outside the resolvable range, for temperatures between 293.2 and 338.2 K. Thus, it is possible that there are either long time constants that are being missed at either lower or higher temperatures (or both), or that there are

TABLE 11: Time-Dependent Anisotropy Parameters Obtained for $Pyrr_{1(2O2)}^+/NTf_2^-$ vs Temperature[a]

T	η	$r(0)$	r_1	$\tau_{1,rot}$	r_2	$\tau_{2,rot}$	r_3	$\tau_{3,rot}$	$\tau_{0,rot}$	$\tau_{1/e,rot}$	$\langle\tau\rangle_{rot}$	$\chi_{red.}^2$
278.2	142.5	0.402	0.0453	0.884	0.245	8.73 (235)	0.112	121 (3260)	5.02	14.1	39.2	1.051
293.2	65.77	0.358	0.0537	0.609	0.250	4.15 (255)	0.0543	439 (27 000)	2.41	4.81	69.7	1.067
308.2	35.45	0.332	0.0539	0.410	0.240	2.10 (252)	0.0382	436 (52 400)	1.35	2.20	51.8	1.064
323.2	21.39	0.327	0.0372	0.209	0.245	1.14 (238)	0.0447	858 (180 000)	0.833	1.32	118	1.035
338.2	14.04	0.342	0.0594	0.185	0.232	0.745 (248)	0.0505	497 (165 000)	0.541	0.82	74.0	1.059
353.2	9.836	0.239	0.0497	0.190	0.189	0.505 (250)			0.376	0.41	0.440	1.105

[a] Temperatures are in K, viscosities η in cP, and Time constants $\tau_{i,rot}$ in ns. The numbers in parentheses in the $\tau_{2,rot}$ and $\tau_{3,rot}$ columns are effective molecular volumes in units of A^3 calculated from eq 8. $\chi_{red.}^2$ is the reduced chi-squared value from the nonlinear least-squares fit.

TABLE 12: VTF and Arrhenius Parameters Obtained by Fitting the C153 TDFSS Time Constants τ_0, $\tau_{1/e}$, and $\langle\tau\rangle$ vs Temperature[a]

		VTF				Arrhenius		
		$\ln(k_0)$	D	T_c	χ^2	$\ln(k_0)$	E_a/R	χ^2
N_{1444}^+/NTf_2^-	τ_0	26.46	−3.805	192.2	1.55	36.65	−5143	1.75
	$\tau_{1/e}$	27.61	−5.645	189.7	0.209	41.77	−7225	0.491
	$\langle\tau\rangle$	27.26	−5.793	186.5	0.0241	40.54	−6896	0.245
N_{6444}^+/NTf_2^-	τ_0	27.54	−8.794	140.2	0.128	33.50	−4122	0.142
	$\tau_{1/e}$	32.50	−32.38	93.86	0.0805	38.54	−6249	0.0740
	$\langle\tau\rangle$	34.03	−71.92	55.86	0.0698	37.47	−5977	0.0588
$Pyrr_{14}^+/NTf_2^-$	τ_0	27.09	−12.80	106.7	0.0333	30.58	−3176	0.0324
	$\tau_{1/e}$	30.54	−35.29	72.17	0.0244	33.74	−4322	0.0252
	$\langle\tau\rangle$	32.35	−74.26	47.45	4.14	34.91	−4961	4.01
$Pyrr_{1(2O2)}^+/NTf_2^-$	τ_0	26.52	−7.490	138.3	0.000278	31.32	−3376	0.0144
	$\tau_{1/e}$	27.01	−6.912	156.5	0.0426	34.15	−4428	0.0767
	$\langle\tau\rangle$	27.65	−87.25	32.97	16.2	29.08	−3671	16.1

[a] Units of T_c and E_a/R are in K, and k_0 units are in s^{-1}. χ^2 values from the nonlinear least-squares fits are not normalized.

nanostructural changes occurring in these liquids with changes in temperature that affect the reorientation time constants.

Because of the possibility that we may be unable to resolve very slow reorientational dynamics of the C153 probe that are nonetheless present, we present the data by analogy with the method used to characterize the TDFSS data above. We have also calculated the effective averaged inverse rate, τ_0, the effective time constant for the 1/e point in the decay, $\tau_{1/e}$, and the average time constant, $\langle\tau\rangle$. In this way, we can compare the dynamics for the six temperatures and four liquids without consideration of whether a 2- or 3-exponential model best fits the C153 fluorescence anisotropy data. Using the three effective time constants τ_0, $\tau_{1/e}$, and $\langle\tau\rangle$ to describe the C153 orientational relaxation, the four ILs can now be analyzed according to three simple models: the Arrhenius, VTF and the Stokes−Einstein−Debye models. Results from these comparisons between models will depend much less strongly on the number of exponential components used to fit the data.

Arrhenius and VTF Analysis of the C153 Reorientation Dynamics. Results obtained by fitting the C153 anisotropy time constants for the four ILs to the Arrhenius and VTF equations are shown in Table 12. The values of $\langle\tau\rangle$ for the pyrrolidinium liquids $Pyrr_{14}^+/NTf_2^-$ and $Pyrr_{1(2O2)}^+/NTf_2^-$ are biased by the longest time constants τ_3 or τ_4, which are beyond our long-time resolution. We have fit the natural log of each of the time constants τ_0, $\tau_{1/e}$, and $\langle\tau\rangle$ to an Arrhenius function $\ln(k) = \ln(k_0) - E_a/(RT)$, and to a VTF function, eq 7. It is apparent on considering the raw values of χ^2 that the VTF equation generally provides a better fit than the Arrhenius equation. Nonetheless, it is useful to consider the range of activation energies obtained for the Arrhenius equation. As would be expected for comparing any faster vs slower process in the condensed phase of the same system, the activation energies E_a are lower for τ_0 than for either $\tau_{1/e}$ or $\langle\tau\rangle$. The activation energies are higher for the tetraalkylammonium ILs than for either $Pyrr_{14}^+/NTf_2^-$ or $Pyrr_{1(2O2)}^+/NTf_2^-$. For the former pair, the E_a values range from 8 to 14 kcal/mol, whereas for the latter, they are in the range from 7 to 10 kcal/mol. The key parameter that is obtained from the VTF analysis is the critical temperature T_c. The values obtained for N_{1444}^+/NTf_2^- are typical for a number of ILs and glassy fluids. The values of T_c are substantially smaller for the other three liquids, indicating that these dynamics are in a regime closer to the Arrhenius or high-temperature limit. We note that the C153 orientational dynamics in $Pyrr_{14}^+/NTf_2^-$ show nearly identical quality fits to either the VTF or the Arrhenius models.

C153 Reorientation Dynamics: Both Microviscosities and Nanostructures. For the simplest case of a spherical rotor, hydrodynamic models often lead to surprisingly accurate predictions for the reorientation dynamics. C153 has been extensively compared with various dressed hydrodynamic models by Maroncelli and co-workers.[57,105] At the simplest level of hydrodynamic theory, the Stokes−Einstein−Debye equation relates the observed time constant for reorientation to the product of the macroscopic shear viscosity, the molecular volume of the reorienting probe molecule, and the inverse absolute temperature. The data from Table 12 for each of the four ionic liquids N_{1444}^+/NTf_2^-, N_{6444}^+/NTf_2^-, $Pyrr_{14}^+/NTf_2^-$ and $Pyrr_{1(2O2)}^+/NTf_2^-$ are plotted in Figure 9. The molecular volume is the same for each case; so we graph the three averaged time constants τ_0, $\tau_{1/e}$, and $\langle\tau\rangle$ vs the ratio of the shear viscosity to temperature, η/T. Because the longest effective time constants $\langle\tau\rangle$ are well beyond our resolvable time window for most of

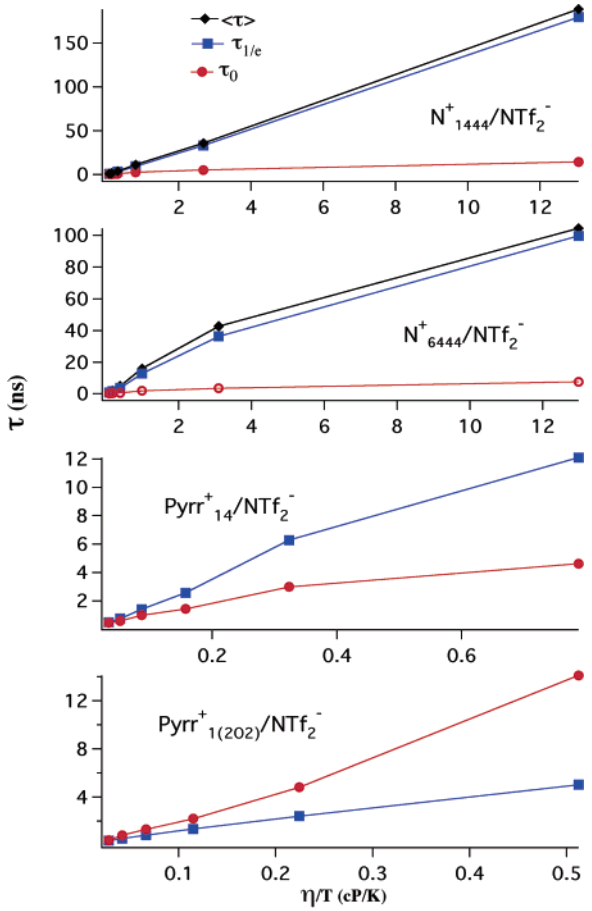

Figure 9. Fluorescence anisotropy effective time constants (in units of ns) τ_0, $\tau_{1/e}$, and $\langle\tau\rangle$ plotted vs the ratio of viscosity over temperature (in units of cP/K) for the ILs N_{1444}^+/NTf_2^-, N_{6444}^+/NTf_2^-, $Pyrr_{14}^+/NTf_2^-$, and $Pyrr_{1(2O2)}^+/NTf_2^-$.

the observed temperatures in $Pyrr_{14}^+/NTf_2^-$ and $Pyrr_{1(2O2)}^+/NTf_2^-$, these data points are omitted from the graphs in Figure 9.

The data shown in Figure 9 are quite intriguing. Qualitatively one might expect to see similar behavior for C153 reorientation dynamics when comparing the ammonium cation ILs N_{1444}^+/NTf_2^- and N_{6444}^+/NTf_2^- and when comparing the pyrrolidinium cation ILs $Pyrr_{14}^+/NTf_2^-$ and $Pyrr_{1(2O2)}^+/NTf_2^-$. However, there is a difference in curvature for the graphs in each case. The estimated molecular volume of C153 is 246 Å^3.[57,81] Because we know the precise sample temperatures and have measured the shear viscosities, we can learn some additional things about the nature of the probe reorientation by considering the Stokes−Einstein−Debye equation that relates the observed reorientation time constant τ_{or} to the shear viscosity η, the molecular volume of the reorienting species V, and the absolute temperature by[57]

$$\tau_{or} = \frac{\eta V}{k_B T} \tag{8}$$

for a model spherical rotor with stick boundary condtions. By using the molecular volume, one can estimate the effective local viscosity from the measured time constants for reorientation. For the data measured at 278.2 K, the viscosities calculated from the first and second reorientation time constants τ_1 (and τ_2) range from about 10−15 cP and 100−160 cP for the N_{1444}^+/NTf_2^- and N_{6444}^+/NTf_2^- ILs, while the measured shear viscosities are over 3600 cP for this temperature. This is clear evidence for reduced local friction, or to use the term from the polymer and aggregate research community, microviscosity. For example, the overall (macroscopic) friction of polymer chains flowing in solution can be quite large as a result of entanglement, whereas very local effects can permit friction (as measured by spectroscopic probes) to be much smaller, more like normal solution viscosities. A similar effect, but less pronounced in relative magnitude is observed for the other two pyrrolidinium ILs. At 278.2 K, the calculated microviscosity values for τ_1 are 7 and 4 cP, for $Pyrr_{14}^+/NTf_2^-$ and $Pyrr_{1(2O2)}^+/NTf_2^-$, respectively. For the former IL, τ_2 leads to an intermediate microviscosity value of 33 cP. Similar microviscosity effects are noticeable for the other five temperatures in all four of the ILs studied. For N_{1444}^+/NTf_2^- and N_{6444}^+/NTf_2^-, the values of the reorientation time constants τ_3 are remarkably close to the values predicted from the measured shear viscosities. Similar results are observed for $Pyrr_{1(2O2)}^+/NTf_2^-$ for the second reorientation time constant τ_2. These results indicate that the reorientational dynamics giving rise to this time constant are governed by frictional forces that can be well described by standard hydrodynamic models for Brownian motion in solution.[57]

For the two pyrrolidinium cation ILs, additional time constants are observed that are substantially longer than would be predicted based on measured shear viscosities and known C153 molecular volume. Time constants for reorientational dynamics on molecular length scales are only observed to increase in this way when the reorienting chromophore is attached to a larger molecular object, as in the case of a probe chromophore attached to a protein.[54−55] Instead of calculating microviscosities, it is appropriate to instead use the SED eq 8 to estimate the molecular volume of the reorienting species. These effective molecular volumes are given in Tables 8−11, listed in parentheses below the relevant time constants. The effective volumes are listed for τ_3 in N_{1444}^+/NTf_2^-, N_{6444}^+/NTf_2^- and $Pyrr_{14}^+/NTf_2^-$, and for τ_4 in $Pyrr_{14}^+/NTf_2^-$ and for τ_2 and τ_3 in $Pyrr_{1(2O2)}^+/NTf_2^-$. The estimated molecular volumes obtained from τ_4 for $Pyrr_{14}^+/NTf_2^-$ are rather large for three of the six temperatures: 293.2, 308.2, and 338.2 K. For these temperatures, the effective volumes range from 7500 to 17 700. The anomalous effective volumes estimated from the values of τ_3 for $Pyrr_{1(2O2)}^+/NTf_2^-$ range from 3300 to 179 000 for the lowest five temperatures.

These large effective volumes suggest that some form of long-range order may exist in these two pyrrolidinium ILs that does not manifest itself in either N_{1444}^+/NTf_2^- or N_{6444}^+/NTf_2^-. Although no liquid-phase structural studies have been reported on the liquids we have studied here, crystal structure data on related materials gives support for this possibility. Choudhury, et al.[106] used cryogenic zone refinement to determine the crystal structure of $Pyrr_{14}^+/NTf_2^-$ at 130 K, and Forsyth and coworkers[30] reported the room-temperature structure of dimethylpyrrolidinium NTf_2^-, which melts at 405 K. Both structures contain sheets, or planes, of NTf_2^- anions and pyrrolidinium cations, so that the environment is not isotropic in all directions. By contrast, the structure of tetrapropylammonium NTf_2^-, which was also reported by Forsyth et al.,[30] shows a type of structure where each cation is surrounded by six cations and vice versa, providing a more isotropic environment. In molecular solvents, crystal and liquid structures usually bear little relation to each other, however, in ionic liquids, the electrostatic forces favor the retention of charge lattices, even if disordered. If sheet-like structural domains persist in the molten pyrrolidinium salts, they could place constraints on the orientational freedom of coumarin 153, similar to the situation in liquid crystalline materials and giving rise to very long-lived components in the fluorescence

anisotropy decay that reflect the reorientation (or restructuring) of larger aggregate structures. This type of longer-range order may not be present in the tetraalkylammonium NTf_2^- salts we have studied here.

There have been a number of recent reports about the nanostructural organization in ionic liquids from molecular dynamics computer simulations. Lopes and Padua discussed results from simulations on 1-alkyl-3-methylimidazolium ILs with both PF_6^- and NTf_2^- anions. Substantial microphase separation was observed, with alkyl tails segregated away from cationic groups and anions.[107] Wang and Voth discussed a related spatial inhomogeneity observed in coarse-grained simulations of the IL *N*-butyl-*N*-methylimidazolium nitrate.[4] A most intriguing report has been made by Shigeto and Hamaguchi on the use of spatially resolved CARS signals to determine that there are persistent aggregates present in ILs with diameters in the tens of nanometers range.[108] The X-ray scattering results of Triolo et al.[34] present convincing evidence for nanostructural organization in ILs with alkylmethyl-imidazolium cations paired with either chloride or BF_4^-. Our observation of anomalously long time constants for reorientation of C153 is made possible only by careful analysis of the fluorescence polarization anisotropy data, which in turn may be providing a subtle hint of heterogeneous clustering or aggregation in these ILs with nonaromatic cations.

Conclusions

We have made detailed studies of the physical and chemical properties of four ionic liquids, N_{1444}^+/NTf_2^-, N_{6444}^+/NTf_2^-, $Pyrr_{14}^+/NTf_2^-$, and $Pyrr_{1(2O2)}^+/NTf_2^-$. Using the solvatochromic fluorescence probe C153, we have studied the temperature dependence of the solvation dynamics and fluorescence depolarization dynamics in the four ionic liquids. To further interpret our fluorescence results, we carried out several other experiments. Using steady-state spectroscopy, we have characterized the local polarity in the vicinity of the solvatochromic probe molecule. For testing whether hydrodynamic models may apply to ionic liquid dynamics, we measured the temperature-dependent viscosities of the four liquids. We used differential scanning calorimetry to characterize the complex phase behavior of the ionic liquids.

Our temperature-dependent studies permit us to draw the following conclusions regarding our four ILs that have nonaromatic cations. The viscosities can be fit to high precision using the VTF model. The DSC results show that the two tetraalkylammonium-cation liquids N_{1444}^+/NTf_2^- and N_{6444}^+/NTf_2^- are supercooled at room temperature, but that the two pyrrolidinium cation ILs are not.

The solvation behavior of these four ILs with nonaromatic cations are nearly fully resolved with the TCSPC fluorescence methods used to measure the C153 emission shifts. The observed solvation dynamics occur on timescales orders of magnitude longer than for most organic solvents. These results will enable a greater understanding of the dynamics of solvated electrons,[77] electron-transfer reactions, and how reactivity in ILs is generally different than in common neutral organic solvents.

The reorientational dynamics of the C153 probe are quite complex. For the N_{1444}^+/NTf_2^- and N_{6444}^+/NTf_2^- liquids, fast orientational time constants provide a clear indication of microviscosities that are orders of magnitude below the measured shear viscosities. The same is also observed for the $Pyrr_{14}^+/NTf_2^-$ and $Pyrr_{1(2O2)}^+/NTf_2^-$ liquids. In addition, there is convincing evidence for rather long orientational time constants that provide evidence for either complex nanostructural reorganization, or embedding of the C153 probe in rather large ion clusters. Though the longest C153 reorientation time constants in the 400−800 ns range have large uncertainties, we are confident that these results do indicate the presence of either the reorganization time scale of some local structure on the nanoscale, or of the reorientation of C153 entrapped within a larger cluster or aggregate comprised of the ionic components of the liquid.

Much work remains to be done to unravel the complexities of both the dynamics and nanostructural organization of these and all ionic liquids. It will be helpful in the future to combine experiments and theory, and to use a broad range of spectroscopic and structural methods to study the liquids. For example, combining singlet and triplet emission probes will permit studies of solvation dynamics and orientational friction from supercooled states to high-temperature states at which the ILs begin to behave more like common organic solvents. Combining NMR diffusion, femtosecond Kerr effect and other nonlinear optical methods, two-dimensional IR spectroscopy experiments, and with neutron and X-ray diffraction and scattering methods will be required to more fully understand these liquids. Because of their great potential for a wide variety of applications, it will be worth the effort.

Acknowledgment. We gratefully acknowledge support for this work from the NSF, the DOE, and the Donors of the Petroleum Research Fund. Work done at Rutgers was supported by the National Science Foundation Grant No. CHE-0239390 and ACS-PRF Grant 42375-AC6. Work at Brookhaven National Laboratory was supported under Contract No. DE-AC02-98CH10886 with the U.S. Department of Energy and supported by its Division of Chemical Sciences, Office of Basic Energy Sciences. Support from the BNL LDRD Program Project No. 03-118 is acknowledged. We thank Dr. Pedatsur Neta (NIST) for his generous provision of the N_{1444}^+/NTf_2^- and N_{6444}^+/NTf_2^-. We thank Benjamin Lee, Jason Giurleo, Jeremy Pronchik, Troy Messina, and David Talaga for their contributions to Igor Pro anisotropy fitting code.

Supporting Information Available: This material is available free of charge via the Internet at http://pubs.acs.org.

References and Notes

(1) Hardacre, C.; Holbrey, J. D.; McMath, S. E. J.; Bowron, D. T.; Soper, A. K. *J. Chem. Phys.* **2003**, *118*, 273−278.
(2) Hamaguchi, H.; Ozawa, R. *Adv. Chem. Phys.* **2005**, *131*, 85−104.
(3) Del Popolo, M. G.; Voth, G. A. *J. Phys. Chem. B* **2004**, *108*, 1744−1752.
(4) Wang, Y. T.; Voth, G. A. *J. Am. Chem. Soc.* **2005**, *127*, 12192−12193.
(5) Lopes, J. N. C.; Padua, A. A. H. *J. Phys. Chem. B* **2006**, *110*, 3330−3335.
(6) Samanta, A. *J. Phys. Chem. B* **2006**, *110*, 13704−13716.
(7) Karmakar, R.; Samanta, A. *J. Phys. Chem. A* **2002**, *106*, 4447−4452.
(8) Karmakar, R.; Samanta, A. *J. Phys. Chem. A* **2002**, *106*, 6670−6675.
(9) Ingram, J. A.; Moog, R. S.; Ito, N.; Biswas, R.; Maroncelli, M. *J. Phys. Chem. B* **2003**, *107*, 5926−5932.
(10) Cang, H.; Li, J.; Fayer, M. D. *J. Chem. Phys.* **2003**, *119*, 13017−13023.
(11) Karmakar, R.; Samanta, A. *J. Phys. Chem. A* **2003**, *107*, 7340−7346.
(12) Ito, N.; Arzhantsev, S.; Heitz, M.; Maroncelli, M. *J. Phys. Chem. B* **2004**, *108*, 5771−5777.
(13) Saha, S.; Mandal, P. K.; Samanta, A. *Phys. Chem. Chem. Phys.* **2004**, *6*, 3106−3110.
(14) Mandal, P. K.; Samanta, A. *J. Phys. Chem. B* **2005**, *109*, 15172−15177.
(15) Ito, N.; Richert, R. *J. Phys. Chem. B* **2007**, *111*, 5016−5022.

(16) Halder, M.; Headley, L. S.; Mukherjee, P.; Song, X.; Petrich, J. W. *J. Phys. Chem. A* **2006**, *110*, 8623−8626.
(17) Mukherjee, P.; Crank, J. A.; Halder, M.; Armstrong, D. W.; Petrich, J. W. *J. Phys. Chem. A* **2006**, *110*, 10725−10730.
(18) Sanders Headley, L.; Mukherjee, P.; Anderson, J. L.; Ding, R.; Halder, M.; Armstrong, D. W.; Song, X.; Petrich, J. W. *J. Phys. Chem. A* **2006**, *110*, 9549−9554.
(19) Arzhantsev, S.; Jin, H.; Ito, N.; Maroncelli, M. *Chem. Phys. Lett.* **2006**, *417*, 524−529.
(20) Li, J.; Wang, I.; Fruchey, K.; Fayer, M. D. *J. Phys. Chem. A* **2006**, *110*, 10384−10391.
(21) Bonhote, P.; Dias, A. P.; Papageorgiou, N.; Kalyanasundaram, K.; Gratzel, M. *Inorg. Chem.* **1996**, *35*, 1168−1178.
(22) Larive, C. K.; Lin, M. F.; Kinnear, B. S.; Piersma, B. J.; Keller, C. E.; Carper, W. R. *J. Phys. Chem. B* **1998**, *102*, 1717−1723.
(23) Seddon, K. R.; Stark, A.; Torres, M. J. *Pure Appl. Chem.* **2000**, *72*, 2275−2287.
(24) Noda, A.; Hayamizu, K.; Watanabe, M. *J. Phys. Chem. B* **2001**, *105*, 4603−4610.
(25) Seddon, K. R.; Stark, A.; Torres, M. J. *ACS Symp. Ser.* **2002**, *819*, 34−49.
(26) Tokuda, H.; Hayamizu, K.; Ishii, K.; Susan, M.; Watanabe, M. *J. Phys. Chem. B* **2005**, *109*, 6103−6110.
(27) Earle, M. J.; Esperanca, J. M. S. S.; Gilea, M. A.; Lopes, J. N. C.; Rebelo, L. P. N.; Magee, J. W.; Seddon, K. R.; Widegren, J. A. *Nature (London, U. K.)* **2006**, *439*, 831−834.
(28) Noda, A.; Susan, A. B.; Kudo, K.; Mitsushima, S.; Hayamizu, K.; Watanabe, M. *J. Phys. Chem. B* **2003**, *107*, 4024−4033.
(29) Every, H.; Bishop, A. G.; Forsyth, M.; MacFarlane, D. R. *Electrochim. Acta* **2000**, *45*, 1279−1284.
(30) Forsyth, C. M.; MacFarlane, D. R.; Golding, J. J.; Huang, J.; Sun, J.; Forsyth, M. *Chem. Mater.* **2002**, *14*, 2103−2108.
(31) Sun, J.; Forsyth, M.; MacFarlane, D. R. *J. Phys. Chem. B* **1998**, *102*, 8858−8864.
(32) Endres, F. *Z. Phys. Chem.* **2004**, *218*, 255−283.
(33) Wang, Y. T.; Izvekov, S.; Yan, T. Y.; Voth, G. A. *J. Phys. Chem. B* **2006**, *110*, 3564−3575.
(34) Triolo, A.; Russina, O.; Bleif, H.-J.; Di Cola, E. *J. Phys. Chem. B* **2007**, *111*, 4641−4644.
(35) Hayashi, S.; Ozawa, R.; Hamaguchi, H. *Chem. Lett.* **2003**, *32*, 498−499.
(36) Ozawa, R.; Hayashi, S.; Saha, S.; Kobayashi, A.; Hamaguchi, H. *Chem. Lett.* **2003**, *32*, 948−949.
(37) Giraud, G.; Gordon, C. M.; Dunkin, I. R.; Wynne, K. *J. Chem. Phys.* **2003**, *119*, 464−477.
(38) Shirota, H.; Castner, E. W., Jr. *J. Phys. Chem. A* **2005**, *109*, 9388−9392.
(39) Shirota, H.; Funston, A. M.; Wishart, J. F.; Castner, E. W., Jr. *J. Chem. Phys.* **2005**, *122*, 184512−1−12.
(40) Shirota, H.; Wishart, J. F.; Castner, E. W., Jr. *J. Phys. Chem. B* **2007**, *111*, 4819−4829.
(41) Holbrey, J. D.; Reichert, W. M.; Rogers, R. D. *Dalton Trans.* **2004**, *15*, 2267−2271.
(42) Castriota, M.; Caruso, T.; Agostino, R. G.; Cazzanelli, E.; Henderson, W. A.; Passerini, S. *J. Phys. Chem. A* **2005**, *109*, 92−96.
(43) Cang, H.; Li, J.; Novikov, V. N.; Fayer, M. D. *J. Chem. Phys.* **2003**, *119*, 10421−10427.
(44) Hyun, B. R.; Dzyuba, S. V.; Bartsch, R. A.; Quitevis, E. L. *J. Phys. Chem. A* **2002**, *106*, 7579−7585.
(45) Rajian, J. R.; Li, S. F.; Bartsch, R. A.; Quitevis, E. L. *Chem. Phys. Lett.* **2004**, *393*, 372−377.
(46) Shirota, H.; Castner, E. W., Jr. *J. Phys. Chem. B* **2005**, *109*, 21576−21585.
(47) Xiao, D.; Rajian, J. R.; Li, S. F.; Bartsch, R. A.; Quitevis, E. L. *J. Phys. Chem. B* **2006**, *110*, 16174−16178.
(48) Asaki, M. L. T.; Redondo, A.; Zawodzinski, T. A.; Taylor, A. J. *J. Chem. Phys.* **2002**, *116*, 10377−10385.
(49) Yamamoto, K.; Tani, M.; Hangyo, M. *The Joint 30th International Conference on Infrared and Millimeter Waves (IEEE Cat. No. 05EX1150)*; IEEE: Hoboken, NJ, 2005; Vol. 2, pp 413−414.
(50) Triolo, A.; Russina, O.; Arrighi, V.; Juranyi, F.; Janssen, S.; Gordon, C. M. *J. Chem. Phys.* **2003**, *119*, 8549−8557.
(51) Triolo, A.; Russina, O.; Hardacre, C.; Nieuwenhuyzen, M.; Gonzalez, M. A.; Grimm, H. *J. Phys. Chem. B* **2005**, *109*, 22061−22066.
(52) Maroncelli, M.; Fleming, G. R. *J. Chem. Phys.* **1987**, *86*, 6221−39.
(53) Horng, M. L.; Gardecki, J. A.; Papazyan, A.; Maroncelli, M. *J. Phys. Chem.* **1995**, *99*, 17311−37.
(54) Valeur, B. *Molecular Fluorescence: Principles and Applications*; Wiley-VCH: New York, 2002.
(55) Lakowicz, J. R. *Principles of Fluorescence Spectroscopy*, 2nd ed.; Kluwer Academic/Plenum Publishers: New York, 1999.
(56) Bialik, C. N.; Wolf, B.; Rachofsky, E. L.; Ross, B. A.; Laws, W. R. *Biophys. J.* **1998**, *75*, 2564−2573.
(57) Horng, M.-L.; Gardecki, J. A.; Maroncelli, M. *J. Phys. Chem. A* **1997**, *101*, 1030−1047.
(58) Arzhantsev, S.; Ito, N.; Heitz, M.; Maroncelli, M. *Chem. Phys. Lett.* **2003**, *381*, 278−286.
(59) Ito, N.; Arzhantsev, S.; Maroncelli, M. *Chem. Phys. Lett.* **2004**, *396*, 83−91.
(60) Chowdhury, P. K.; Halder, M.; Sanders, L.; Calhoun, T.; Anderson, J. L.; Armstrong, D. W.; Song, X.; Petrich, J. W. *J. Phys. Chem. B* **2004**, *108*, 10245−10255.
(61) Lang, B.; Angulo, G.; Vauthey, E. *J. Phys. Chem. A* **2006**, *110*, 7028−7034.
(62) Chakrabarty, D.; Chakraborty, A.; Seth, D.; Sarkar, N. *J. Phys. Chem. A* **2005**, *109*, 1764−1769.
(63) Chakrabarty, D.; Harza, P.; Chakraborty, A.; Seth, D.; Sarkar, N. *Chem. Phys. Lett.* **2003**, *381*, 697−704.
(64) Mandal, P. K.; Sarkar, M.; Samanta, A. *J. Phys. Chem. A* **2004**, *108*, 9048−9053.
(65) Baker, S. N.; Baker, G. A.; Kane, M. A.; Bright, F. V. *J. Phys. Chem. B* **2001**, *105*, 9663−9668.
(66) Baker, S. N.; Baker, G. A.; Munson, C. A.; Chen, F.; Bukowski, E. J.; Cartwright, A. N.; Bright, F. V. *Ind. Eng. Chem. Res.* **2003**, *42*, 6457−6463.
(67) Karmakar, R.; Samanta, A. *Chem. Phys. Lett.* **2003**, *376*, 638−645.
(68) Shim, Y.; Duan, J. S.; Choi, M. Y.; Kim, H. J. *J. Chem. Phys.* **2003**, *119*, 6411−6414.
(69) Kobrak, M. N.; Znamenskiy, V. *Chem. Phys. Lett.* **2004**, *395*, 127−132.
(70) Shim, Y.; Choi, M. Y.; Kim, H. J. *J. Chem. Phys.* **2005**, *122*, 044510.
(71) Shim, Y.; Choi, M. Y.; Kim, H. J. *J. Chem. Phys.* **2005**, *122*, 044511.
(72) Fee, R. S.; Maroncelli, M. *Chem. Phys.* **1994**, *183*, 235−247.
(73) Arzhantsev, S.; Jina, H.; Baker, G.; Maroncelli, M. *J. Phys. Chem. B* **2007**, *111*, 4978−4989.
(74) Bart, E.; Meltsin, A.; Huppert, D. *J. Phys. Chem.* **1995**, *99*, 9253−9257.
(75) Bart, E.; Meltsin, A.; Huppert, D. *J. Phys. Chem.* **1994**, *98*, 10819−10823.
(76) Bart, E.; Meltsin, A.; Huppert, D. *J. Phys. Chem.* **1994**, *98*, 3295−3299.
(77) Funston, A. M.; Wishart, J. F. In *Ionic Liquids IIIA: Fundamentals, Progress, Challenges and Opportunities*; Rogers, R. D., Seddon, K. R., Eds., Vol. 901 of ACS Symp. Ser.; American Chemical Society: Washington, DC, 2005; pp 102−116.
(78) Skrzypczak, A.; Neta, P. *J. Phys. Chem. A* **2003**, *107*, 7800−7803.
(79) Skrzypczak, A.; Neta, P. *Int. J. Chem. Kinet.* **2004**, *36*, 253−258.
(80) Sun, Y.; Castner, E. W., Jr.; Lawson, C. L.; Falkowski, P. G. *FEBS Lett.* **2004**, *570*, 175−183.
(81) Grant, C. D.; Steege, K. E.; Bunagan, M. R.; Castner, E. W., Jr. *J. Phys. Chem. B* **2005**, *109*, 22273−22284.
(82) Grant, C. D.; DeRitter, M. R.; Steege, K. E.; Fadeeva, T. A.; Castner, E. W., Jr. *Langmuir* **2005**, *21*, 1745−1752.
(83) Shirota, H.; Castner, E. W., Jr. *J. Chem. Phys.* **2000**, *112*, 2367−2376.
(84) Frauchiger, L.; Shirota, H.; Uhrich, K. E.; Castner, E. W., Jr. *J. Phys. Chem. B* **2002**, *106*, 7463−7468.
(85) Olano, E. M.; Grant, C. D.; Norman, T. J., Jr.; Castner, E. W., Jr.; Zhang, J. Z. *J. Nanosci. Nanotechnol.* **2005**, *5*, 1492−1497.
(86) Steege, K. E.; Wang, J.; Uhrich, K. E.; Castner, E. W., Jr. *Macromolecules* **2007**, *40*, ma061779l, in press.
(87) Igor pro 5.04b. Wavemetrics Igor Pro 5.04b Edition; Wavemetrics, Inc.: Lake Oswego, OR, 2005.
(88) Cross, A. J.; Fleming, G. R. *Biophys. J.* **1984**, *46*, 45−56.
(89) Becker, W. *Advanced time-correlated single photon counting techniques*; Springer: Berlin, 2005. Vol. xix; p 401.
(90) MacFarlane, D. R.; Meakin, P.; Sun, J.; Amini, N.; Forsyth, M. *J. Phys. Chem. B* **1999**, *103*, 4164−4170.
(91) Xu, W.; Cooper, E. I.; Angell, C. A. *J. Phys. Chem. B* **2003**, *107*, 6170−6178.
(92) Angell, C. A.; Alba, C.; Arzimanoglou, A.; Boehmer, R.; Fan, J.; Lu, Q.; Sanchez, E.; Senapati, H.; Tatsumisago, M. *AIP Conference Proceedings* **1992**, *256*, 3−19.
(93) Angell, C. A. *Chem. Rev. (Washington, DC)* **2002**, *102*, 2627−2649.
(94) Matyushov, D. V.; Newton, M. D. *J. Phys. Chem. A* **2001**, *105*, 8516−8532.
(95) Cave, R. J.; Castner, E. W., Jr. *J. Phys. Chem. A* **2002**, *106*, 12117−12123.
(96) Ingrosso, F.; Mennucci, B.; Tomasi, J. *J. Mol. Liq.* **2003**, *108*, 21−46.

(97) Ingrosso, F.; Ladanyi, B. M.; Mennucci, B.; Elola, M. D.; Tomasi, J. *J. Phys. Chem. B* **2005**, *109*, 3553−3564.
(98) Paul, A.; Mandal, P. K.; Samanta, A. *J. Phys. Chem. B* **2005**, *109*, 9148−9153.
(99) Paul, A.; Mandal, P. K.; Samanta, A. *Chem. Phys. Lett.* **2005**, *402*, 375−379.
(100) Aki, S. N. V. K.; Brennecke, J. F.; Samanta, A. *Chem. Commun. (Cambridge, U.K.)* **2001**, *5*, 413−414.
(101) Fletcher, K. A.; Storey, I. A.; Hendricks, A. E.; Pandey, S. *Green Chem.* **2001**, *3*, 210−215.
(102) Castner, E. W., Jr.; Maroncelli, M.; Fleming, G. R. *J. Chem. Phys.* **1987**, *86*, 1090−7.
(103) Castner, E. W., Jr.; Fleming, G. R.; Bagchi, B.; Maroncelli, M. *J. Chem. Phys.* **1988**, *89*, 3519−34.
(104) Ito, N.; Huang, W.; Richert, R. *J. Phys. Chem. B* **2006**, *110*, 4371−4377.
(105) Reynolds, L.; Gardecki, J. A.; Frankland, S. J. V.; Horng, M. L.; Maroncelli, M. *J. Phys. Chem.* **1996**, *100*, 10337−10354.
(106) Choudhury, A. R.; Winterton, N.; Steiner, A.; Cooper, A. I.; Johnson, K. A. *J. Am. Chem. Soc.* **2005**, *127*, 16792−16793.
(107) Lopes, J. N. C.; Gomes, M. F. C.; Padua, A. A. H. *J. Phys. Chem. B* **2006**, *110*, 16816−16818.
(108) Shigeto, S.; Hamaguchi, H. *Chem. Phys. Lett.* **2006**, *427*, 329−332.